AN ABSTRACT OF THE THESIS OF

Bradley Jameson Reid for the degree of Master of Science in Oceanography presented on 17 October 1986

Title: The Fall Transition of Oregon Shelf Waters

Abstract approved: Redacted for privacy

Adriana Huyer

A long and gradual transition between the summer and winter oceanic regimes was observed off Oregon during the autumn of 1980. Hydrographic sections and a single current meter mooring between August and December show the ocean possessed characteristics during fall that have not been observed during other seasons: a slow ascension of the poleward undercurrent and the appearance of a large bottom boundary layer.

The decay of summer's southward surface flow was achieved by a series of modest northward wind events during late summer as the effects of southward winds were becoming diminished. The northward wind events had progressively stronger influence on surface currents. The barotropic current fluctuations that are a signature of the summer regime

continued during the transitional period. The weekly-to-monthly averaged flow was barotropic during much of the transition.

Hydrographic sections and time series of alongshore current shear and temperature show that the leveling of the frontal layer was achieved gradually over a two month time scale.

The winter regime was established during eleven days of continuous northward wind stress in early November.

The Fall Transition of Oregon Shelf Waters

by

Bradley Jameson Reid

A THESIS

submitted to

Oregon State University

in partial fulfillment of

the requirements for the

degree of

Master of Science

Completed 17 October 1986

Commencement June 1987

APPROVED:

Redacted for privacy

Professor of Oceanography in charge of major

Redacted for privacy

Dean of College of Oceanography

Redacted for privacy

Dean of Graduate School

Date thesis is presented October 17, 1986

Typed by researcher for Bradley Jameson Reid

to Wendy

ACKNOWLEDGEMENTS

Heartfelt appreciation to you, Dr. Adriana Huyer, for your wisdom and support, understanding and patience these three years. I am obliged and very grateful.

The design and much of the data processing for the "Fall Transition Experiment" was already completed when I arrived at OSU. The effort of several people is appreciated: Rich Schramm, Glenna and Henry Pittock for the data processing and Jane Fleischbein for data processing and assistance in figure drafting.

The virtuosity of Dr. Adriana Huyer and Dr. Robert Smith in their artfulness and craft in ocean question asking (and getting answers!) made my task easier, and that is greatly appreciated.

I am indebted to Dr. Dudley Chelton for his excellent computer software - generously given - without which this thesis would have taken much longer and for the comments on an earlier draft of this thesis.

I am grateful to: Dr. Michael Kosro for the excellent comments and suggestions on an earlier draft of this thesis; Jerry Johnson for supplying the complex EOF software; Theresa Paluszkiewicz and Jeffrey Paduan for the eleventh hour discussion; and to Linda Henshaw who read the numbers as I typed them into the computer,

"make me thy lyre even as the ocean is".

This research was supported by the National Science Foundation through grants OCE - 8014943, OCE - 8405232 and OCE - 8410861.

TABLE OF CONTENTS

LIST OF FIGURES

LIST OF TABLES

THE FALL TRANSITION OF OREGON SHELF WATERS

I. INTRODUCTION

The Seasonal Cycle

Strong seasonal signals are prominent phenomena of waters on the Oregon continental shelf. Currents (Huyer et al., 1975), the offshore density field (Huyer, 1977) and sea level (Brunson, 1973) vary with the seasons. Forcing of seasonal oceanographic cycles off Oregon is chiefly due to the migratory behavior of North Pacific High and Aleutian Low pressure systems: poleward in summer and equatorward in winter. Oregon waters come under the influence of a storm-bearing low pressure system during winter and a high pressure system in summer. The Aleutian Low often brings northeastward or north-northeastward winds to Oregon coastal waters; winter wind direction (11 year mean, 1970-1980) at Newport points 4° clockwise of north (Pittock et al.,1982). The North Pacific High brings southeastward winds; summer mean wind direction points 152° clockwise of north. The extremes of the oceanic seasonal cycle occur during summer and winter with spring and fall being the transitional periods between the summer and winter regimes. The emphasis of this

thesis will be to identify, analyze and describe the departure from summer oceanographic conditions and the subsequent establishment of the winter regime on the Oregon continental shelf during autumn, 1980.

Winter and Summer Regimes

Summer and winter oceanographic regimes are very different over the Oregon continental shelf (Huyer et al., 1975; Huyer, 1977; Huyer et al., 1978). In summer, (1) there is a southward coastal jet at the surface, whose maximum is 15-30 km from shore, and which persists even during northward wind fluctuations; (2) there is a mean vertical shear, such that deeper currents are always northward relative to the surface current, and which does not change appreciably during wind-driven current fluctuations; (3) there is a persistent positive lateral density gradient which balances the mean shear, with isopycnals sloping upward toward the coast, even during periods when the wind is unfavorable for upwelling for several days; (4) there is a mean poleward undercurrent along the bottom; (5) the wind-driven fluctuations in the alongshore current are nearly barotropic, i.e., their amplitude is almost independent of depth; (6) a thermocline is present from the surface to 30 m; and (7) surface salinities decrease and temperatures increase with distance from shore.

In contrast, during winter, (1) there is mean northward flow over the entire shelf, and the strongest flow is immediately adjacent to the coast; (2) the vertical shear fluctuates strongly in association with the wind-driven current fluctuations, but its mean is about zero; (3) the lateral density gradient has significant fluctuations, which are in balance with the fluctuating shear, but its mean is near zero, with generally level or downward-sloping isopycnals; (4) there is no identifiable undercurrent over the continental shelf; (5) the wind-driven fluctuations in the alongshore current have a significant baroclinic component, although they are in the same direction throughout the water column; (6) near surface waters are isothermal to 50 m; and (7) surface salinities increase in the offshore direction.

Pacific Northeastern Hydrography

Early research of salinity, temperature and density variations of the Pacific Northeastern coastal water mass showed it was a mixture of Equatorial Pacific and Subarctic waters, with the latter water mass being the major contributor (Sverdrup et al., 1942).

Pacific Northeastern coastal waters can be described as having three zones: the upper zone, the halocline zone and the lower zone (Dodimead et

al., 1963). The upper zone is characterized by low salinities. It usually occurs in the upper 100 m. It has a homogeneous structure during winter months. The halocline zone acts as a buffer between the upper and lower zones. It usually occurs between 100-200 m. Downward mixing of surface waters is limited to the depth of the halocline zone. Within the halocline zone the temperature usually decreases with depth. Below the halocline zone is the lower zone. Within the lower zone salinities increase gradually and uniformly with depth to the bottom. Modified Pacific Subarctic water is found below the halocline. Any changes of water structure in the lower zone are slow and occur on a nonseasonal basis (Tully, 1964).

The frontal layer, or permanent pycnocline, is historically designated as being between the 25.5 and 26.0 sigma-t values; it tilts upward towards the coast during the summer upwelling months (Collins, 1964). Two pycnoclines exist during the upwelling season: the deeper of the two is the permanent pycnocline, while the other pycnocline is shallow, about 20 m deep, and seasonal. The shallower pycnocline is formed by the seasonal thermocline and a halocline derived from Columbia River plume water; it is nearly level, except inshore, where it tends to merge with the permanent pycnocline to form a surface front (Mooers et al., 1976). The

frontal layer may be due to either the halocline or the thermocline, or both of these coinciding. In Pacific Northeastern waters, the thermocline is seasonal while the halocline is permanent and deeper. The lower depths of the frontal layer are due to the permanent halocline, while the upper depths of the frontal layer are due to the halocline and seasonal thermocline.

In general, summer surface temperatures are warmer than winter temperatures, although in the band of upwelling adjacent to the coast, summer temperatures and salinities are cooler and more saline than winter values (Bourke, 1972). Surface waters are 0.5 to 1.0 ‰ more saline in summer than winter and the offshore temperature gradient is four times larger in summer than winter. A halocline is observed in both seasons, extending to 75 m in summer and 100 m in winter.

The Spring Transition

The transition from the winter to the spring-summer regime was observed in detail during the WISP experiment that took place in winter and spring 1975 off Oregon (Huyer et al., 1979). The spring transition occurred in late March during a single upwelling event. Before this event, the vertical shear and the near bottom density showed strong fluctuations but after this event the surface current was persistently more southward

than the bottom current (except for a day or two in May) and the bottom density remained high, as would be the case with persistent upward sloping isopycnals. During this event, the lateral density gradient as observed from moored current meters reached a value greater than during any previous southward events, a value that may have been critical in establishing the persistent vertical shear. The transition was associated with the first major southward wind stress event of the season. Subsequent northward events of the same magnitude, e.g., in early May, were not sufficient for re-establishing the winter regime, and subsequent strong southward events did not cause greatly increased vertical shear or stronger southward near-surface currents. Thus, the spring transition from the typically winter regime with mean northward flow and no mean shear to the typically summer regime with southward surface currents and strong vertical shear occurs with the first major upwelling event of the season.

The Fall Transition

Much data has been collected and analyzed on coastal upwelling and the summer regime (e.g., Smith, 1974; Kundu et al., 1975; Mooers et al., 1976; Halpern, 1976; Kundu and Allen, 1976; Allen and Kundu, 1978). The winter regime has been analyzed by Huyer et al., (1975); Huyer

(1977); and Sobey (1977). The spring transition has been analyzed by Sobey (1977); Huyer et al., (1979); Brink et al., (1984); and Strub et al., (1987).

Less attention has been paid to the autumn transition, when oceanographic conditions change from the summer regime to the winter regime. Burt and Wyatt (1964), from analysis of drifting salad dressing bottle returns between 1959 and 1963, found variable surface currents in September, southward surface currents in August and northward surface currents in October. Wyatt, Burt and Pattullo (1972), in a ten-year study (1961-1971) of bottle returns, concluded that the transitional month of surface currents was September. Sakou and Neshyba (1972), from moored current meters 50 km offshore, found variable surface currents in August and September and northward currents during October. Collins (1968) from current meter measurements over mid-shelf in 1965 found southward near-surface (20 m) currents in late August, variable currents in September and northward currents in October.

Collins (1964), from analysis of hydrographic data, found the density regime to remain inclined upwards towards the coast until late September or October. Huyer (1977) found that geostrophic flow across the Newport line was northward from October through February and

southward from March through September. An index of upwelling, the offshore Ekman transport computed from monthly mean surface atmospheric pressure field, indicates the upwelling season off Oregon usually extends from April through September (Bakun, 1972).

In summary, the transition of shelf surface currents off Oregon has been observed in different years to occur during September. Hydrographic observations generally show September as a month with net upwelling and an inclined frontal layer, and October as month of transition. This would imply that the transition occurs earlier inshore over the shelf than farther offshore. These conclusions are consistent with the results of this thesis.

The Fall Transition Experiment

The experiment was designed to study the autumn transition from summer to winter oceanographic regimes. Answers to the following questions were sought:

(1) How did the southward surface current decay?

   (a) Did it decay very gradually by dissipation? Would it disappear even if there were no northward wind events in late summer and fall?

(b) Did it disappear suddenly, as a result of a single strong northward wind stress event?

(c) Was the southward surface current replaced by northward surface flow in incremental steps through a series of northward wind events which are common in fall?

(2) Did the winter northward flow regime result from the surfacing of the undercurrent?

(3) Was the fall transition achieved primarily by means of a change in the offshore density gradients, as appears to be the case during the spring transition?

(4) Were the current fluctuations associated with the transition primarily barotropic or baroclinic in nature?

In this thesis, we try to answer all of these questions.

II. DESCRIPTION OF THE DATA

The experiment was conducted from 20 August to 2 December 1980. Included in the experiment was a single current meter mooring over the mid-shelf at 45° N (Figures 1 and 2), and, approximately monthly CTD sections were made across the continental margin along 45° N (Figures 1 and 3) (Reid et al., 1985). Supplementary observations of wind speed and direction, sea level and atmospheric pressure were available from Newport, Oregon (Pittock et al., 1982).

CTD Data

Five CTD (*in situ* Conductivity/Temperature/Depth) sections were made between August and December, 1980 along 45° N on the R/V Wecoma (Figures 4 and 5):

Cruise	Date
W8008A	August 20-21
W8009B	September 22-23
W8010B	October 28-30
W8011A	November 17-19
W8012A	December 1-2

Standard station positions (Figure 1) were at 124°03' W (3.1 km

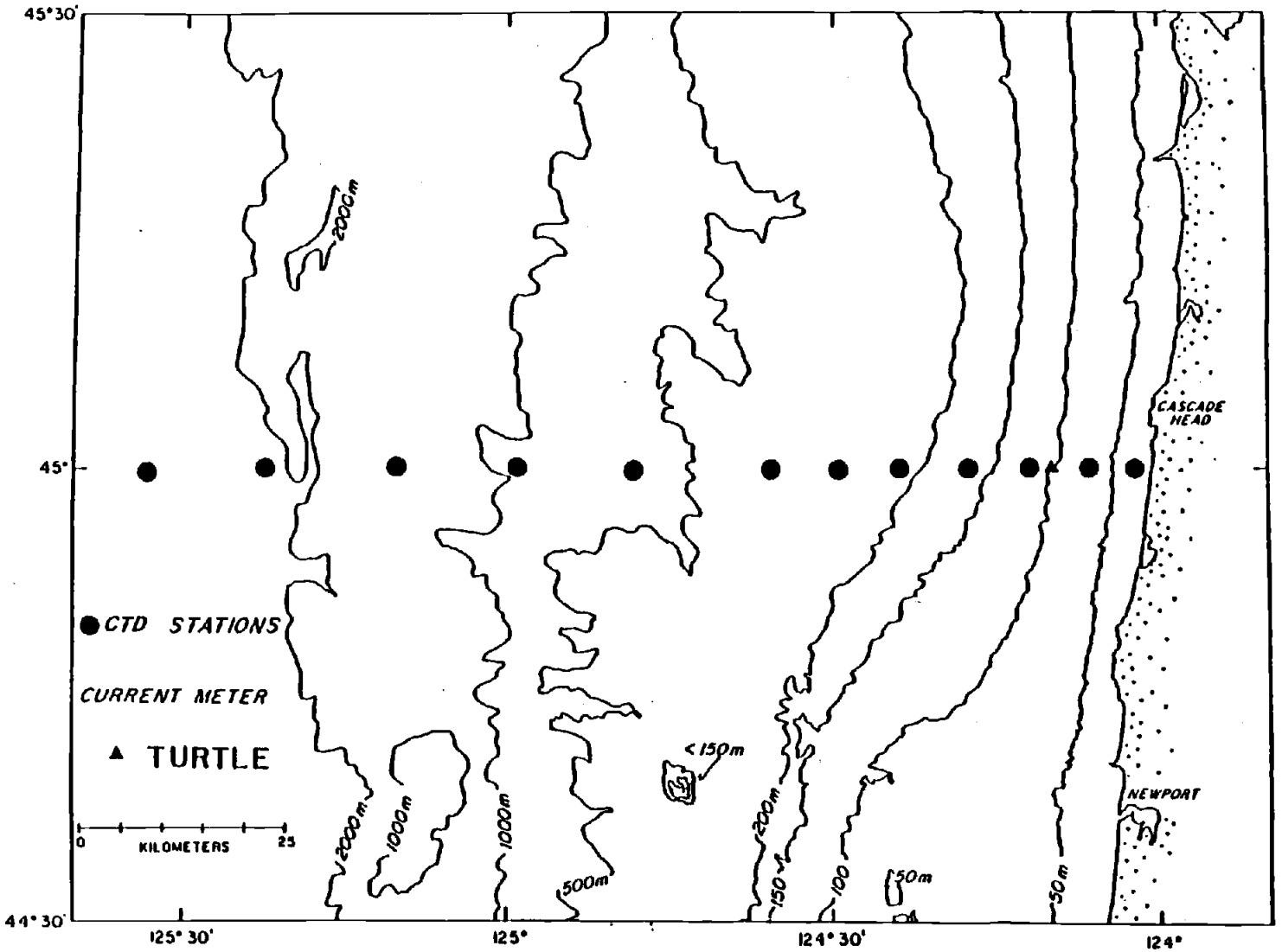

Figure 1. Location of current meter TURTLE and standard CTD station positions.

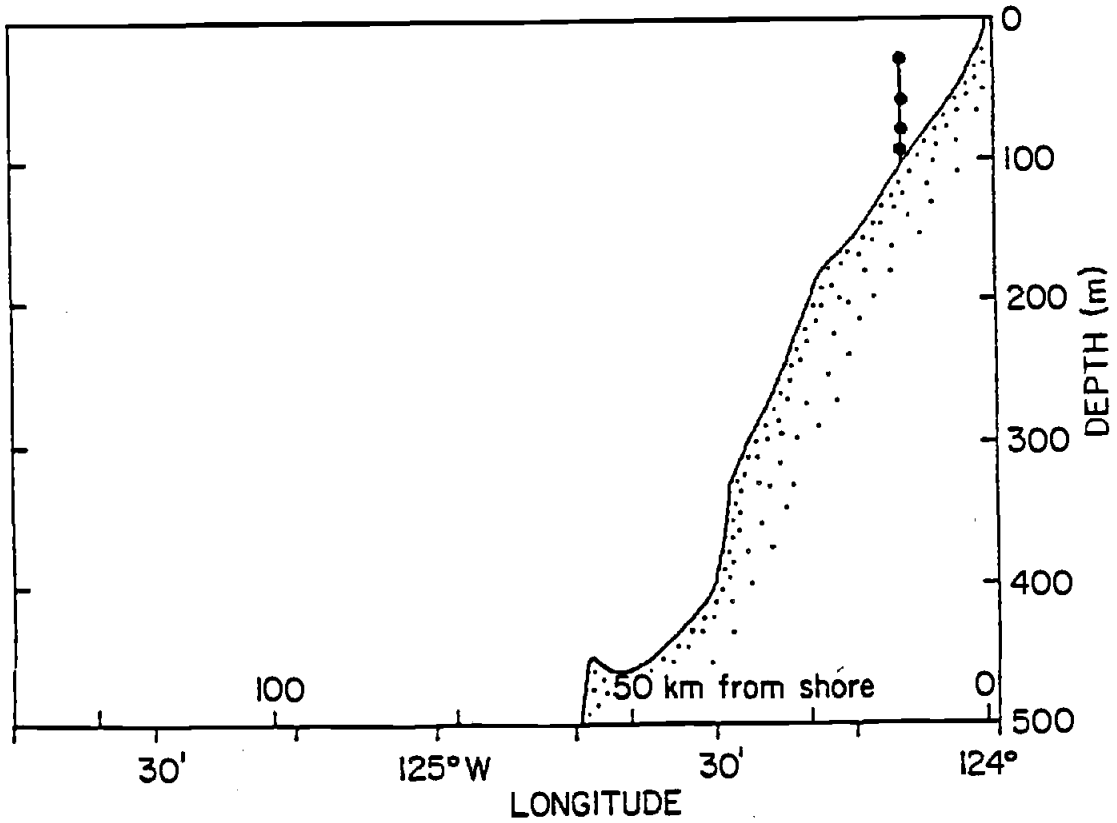

Figure 2. Current meter TURTLE and bottom profile along 45° N.

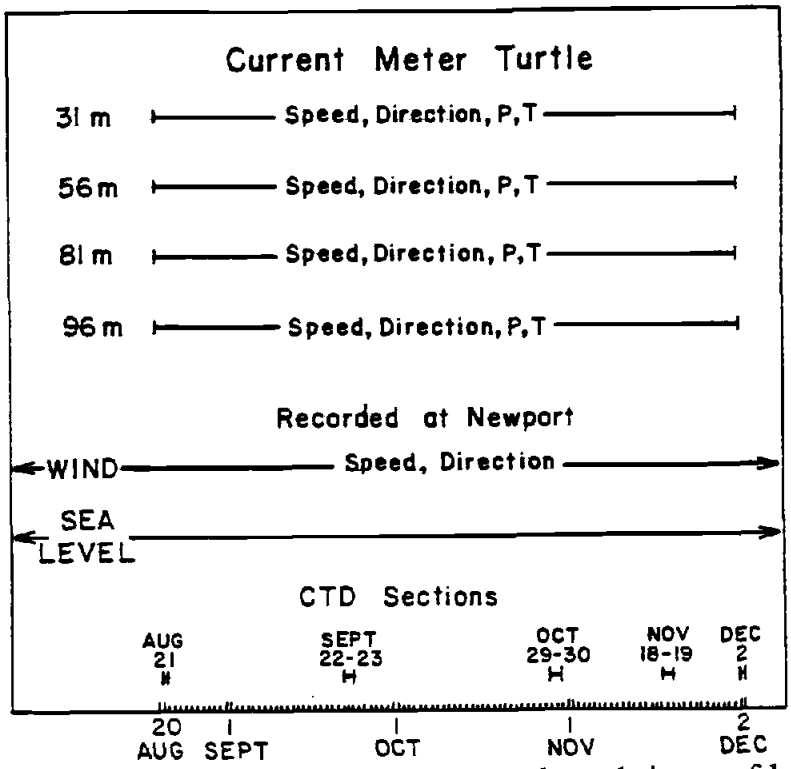

Figure 3. Length of current meter records and times of hydrographic sections along 45° N.

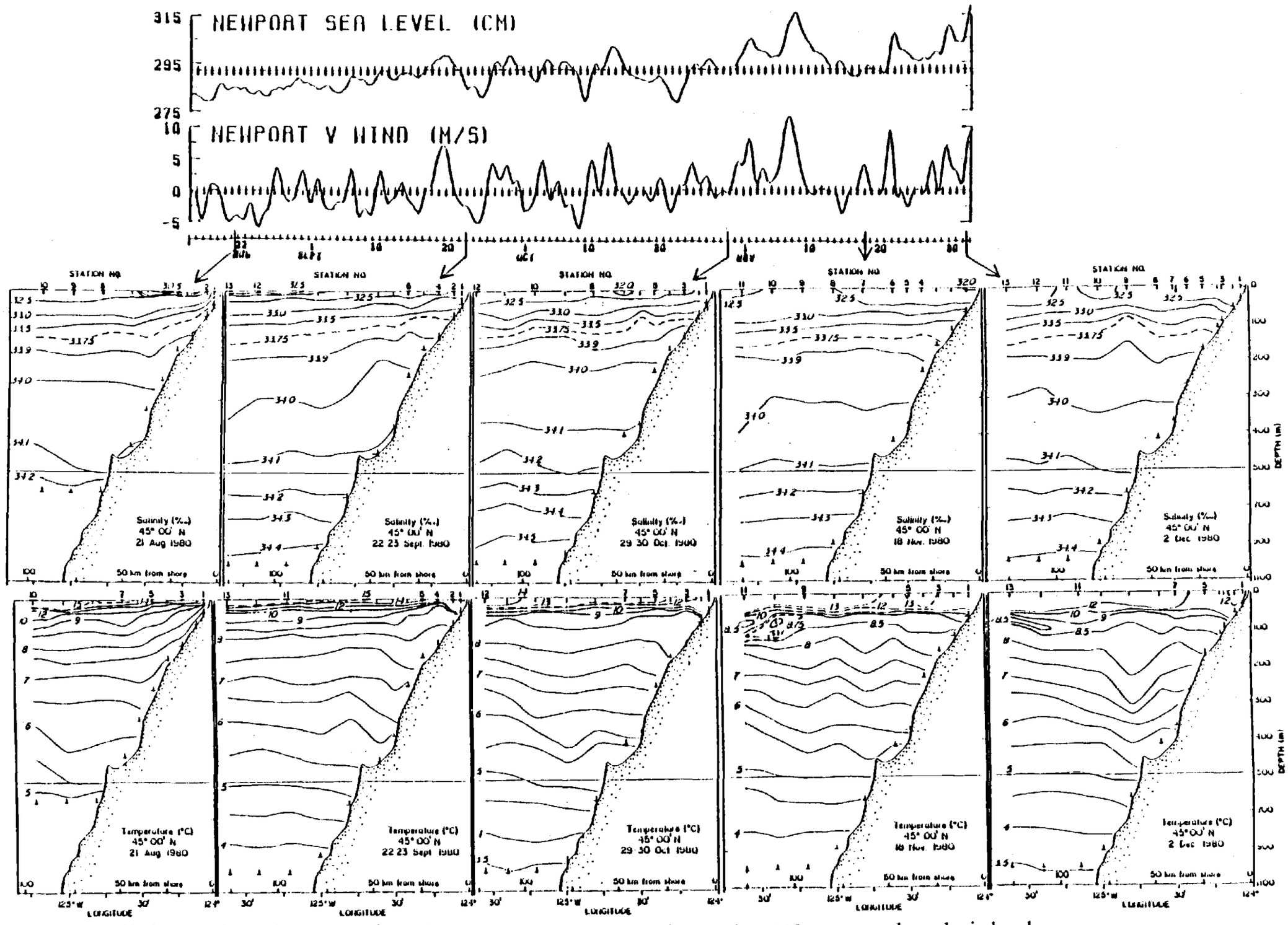

Figure 4. Hydrographic sections of salinity and temperature along 45° N; time series of Newport northward wind and sea level.

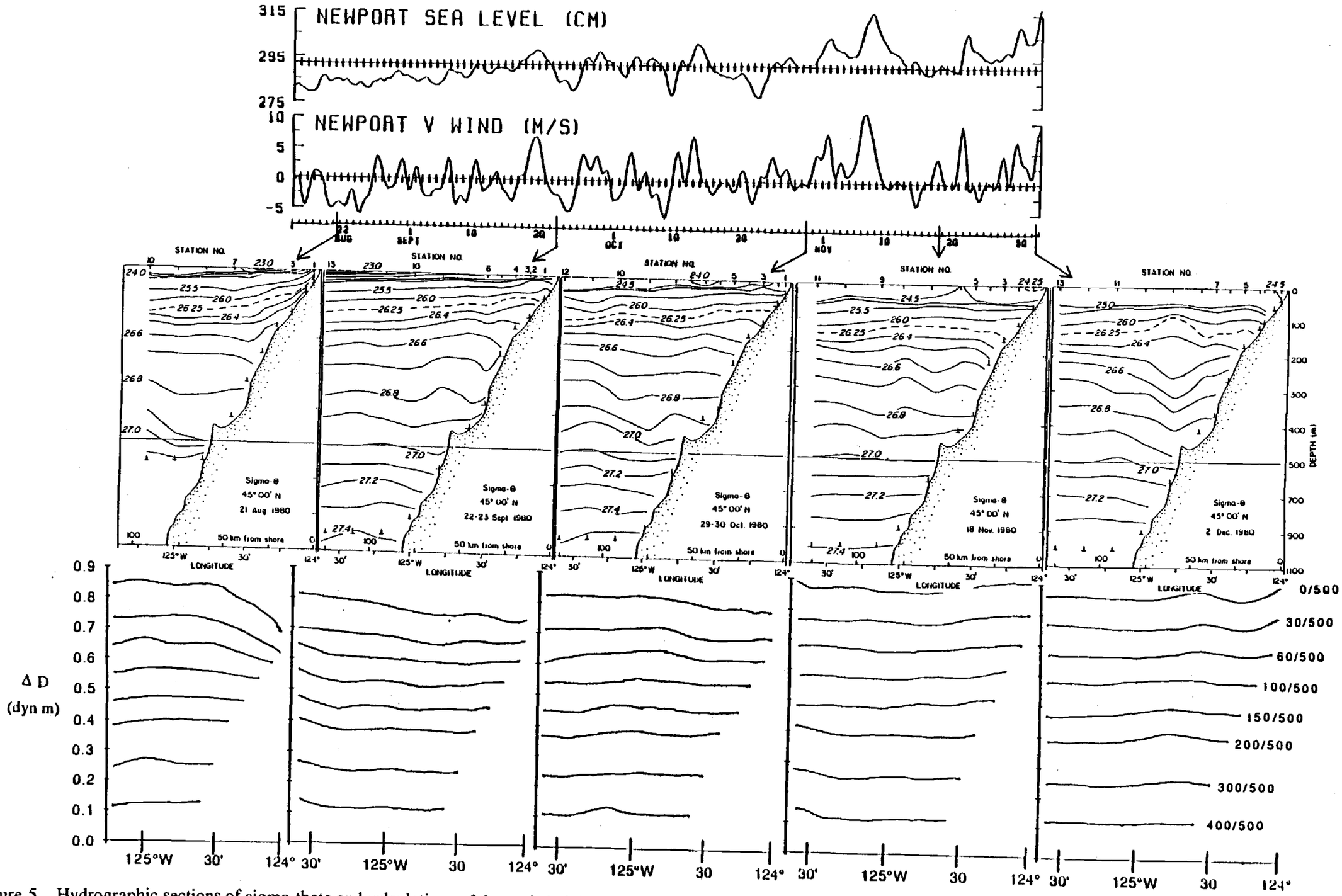

Figure 5. Hydrographic sections of sigma-theta and calculations of dynamic height on selected pressure surfaces along 45° N; time series of Newport northward wind and sea level.

offshore), six minutes of longitude (7.9 km) apart between 124°06' W (6.9 km offshore) and 124°36' W (46.4 km offshore), and twelve minutes (15.7 km) apart between 124°48' W (62.1 km offshore) and 125°36' W (125.2 km offshore). Maximum sampling depth was 600 decibars (db) during the August cruise and 1000 db during all other cruises.

The CTD observations were made with two different types of CTD probes. On the first three cruises, the Geodyne A775 CTD was used. On the last two cruises (W8011A; W8012A), one of the newly acquired Neil Brown Instruments Mark IIIb CTD probes was used. CTD probe calibration and data processing techniques are described in Reid et al., (1985). The accuracy of the Geodyne A775 probe is ±3.0 db for pressure, ±0.02 °C for temperature and 0.03 mmhos cm^{-2} for salinity. The accuracy of the Neil Brown Mark IIIb probe is ±6.5 db for pressure, ±0.005 °C for temperature and 0.005 mmhos cm^{-2} for salinity.

The temperature and salinity fields (Figure 4), and the density field and steric heights along pressure surfaces (Figure 5), observed during the five sections are shown with time series of the northward wind and sea level. These will be discussed in Chapter III. Steric heights (in dynamic meters) at various selected pressure surfaces with respect to the 500 dbar (assumed level) are shown in Figure 5; the method followed, in which the

gradient of steric height was extrapolated into the sea floor, is described in Reid and Mantyla (1976). The calculations of steric height are placed under the sections of sigma-theta to facilitate comparisons.

Current Meter Data

The current meter mooring (designated TURTLE) was located over the 106 meter isobath, 12.5 km offshore of the Oregon coast (Figures 1 and 2), at 44°59.6' N, 124°10.1' W. The mooring was equipped with subsurface flotation at 25 m, and four Aanderaa RCM4 current meters at depths of 31, 56, 81 and 96 m (Figure 2). The mooring was deployed at 2303 GMT on 20 August 1980 and recovered at 2056 GMT on 1 December 1980. Each current meter recorded average speed, and instantaneous direction, temperature, pressure and conductivity. The general calibration and data processing techniques for Aanderaa current meter data have been described by Pillsbury et al. (1974) and Denbo et al. (1984). The compass calibration procedure and compass accuracy for this experiment is described in the Appendix. The accuracy of temperature observations is ±0.05° C (Denbo et al., 1984). The accuracy of the speed sensors (Pillsbury et al., 1974) generally range from 19% at 2 cm/s (±0.4 cm/s), to less than 1% at 30 cm/s (±0.3 cm/s), with a 4% error at 8 cm/s (±0.3 cm/s).

Current meter data were recorded at thirty-minute intervals; the processed data consist of hourly values. The hourly speed and direction data were used to calculate the eastward (u) and northward (v) components. The hourly wind and current meter data are presented in Reid et al., (1985).

Progressive vector diagrams (PVDs) were calculated from the hourly current data at Turtle and the Newport wind (Figure 6). These diagrams are constructed by placing consecutive velocity vectors end-to-end with the initial vector located at the origin. PVDs should not be considered representative of water mass path since current and wind velocities are Eulerian measurements. The axes in Figure 6 are scaled in kilometers. Dividing the length of the total vector on a PVD by the record length (102.9 days) is equal to mean vector velocity. A line drawn from the origin to the last vector drawn points toward mean vector direction. The PVDs show that poleward currents were not strongest at the deepest current meter but at 81 m. Current variations at 96 m seemed to be constrained entirely along an axis parallel to the local isobath. Current flow at 31 m, initially southward, reversed direction during the month of September. The PVD of the Newport wind shows the winds were south-southeastward from late August through September, although there

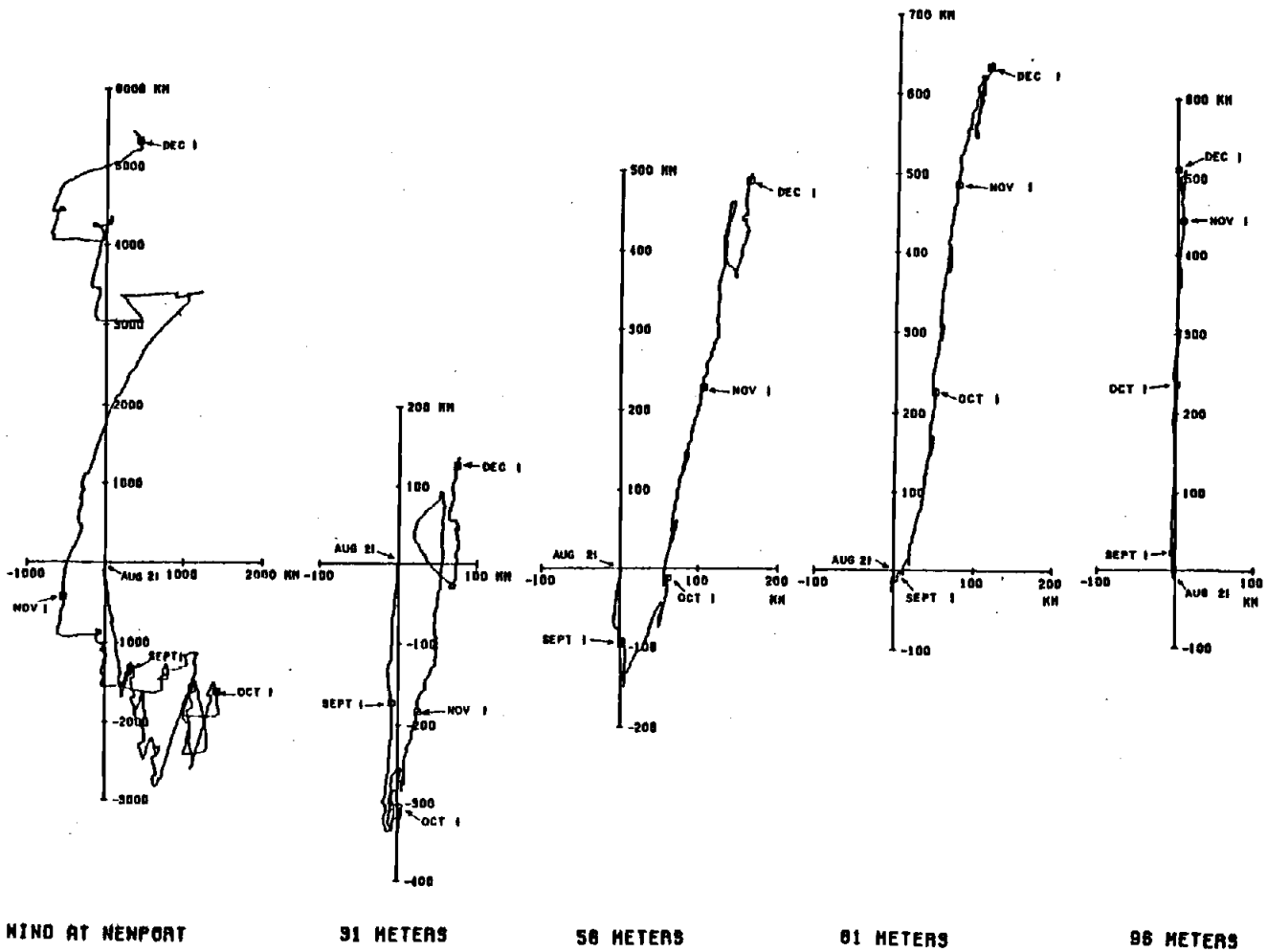

Figure 6. Progressive vector diagrams of currents and wind from hourly data.

were frequent reversals towards north-northeastward. The wind fluctuations continued during October, often rotating clockwise during fluctuations from southward to northward. During November, winds were primarily northeastward.

The atmospheric pressure and sea level records also consist of hourly values. The hourly atmospheric pressure and sea level are presented in Pittock et al., (1982).

The eastward (τ_x) and northward (τ_y) components of wind stress were computed from the eastward (U) and northward (V) components of wind velocity:

$$\tau_x = \rho\, C_D \left(\sqrt{U^2+V^2}\right) U$$
$$\tau_y = \rho\, C_D \left(\sqrt{U^2+V^2}\right) V$$

where τ is in dynes/cm^2,U and V are in cm/s, ρ is air density, taken to be 0.00125 gm cm^{-3}, and C_D is the drag coefficient, taken to be (0.75 +0.067 $\sqrt{U^2+V^2}$)) x 10^{-3} and must be calculated with U and V in m/s (Garratt, 1977).

All hourly time series were subsequently low-passed filtered (using

a filter with a half-power point of 46 hours) to remove tidal and inertial frequency and decimated to a six-hourly data interval. The low-passed sea level data were adjusted for the inverted barometer effect, by which sea level falls one centimeter when atmospheric pressure rises by one millibar; this will be referred to in this thesis as sea level. All time series in this thesis are low-passed data.

Vector time series of the low-passed currents and Newport wind (Figure 7) show that currents were generally directed northward or southward, nearly parallel to the coastline and local isobaths (Figure 1).

The orientation of the principal axes (Fofonoff, 1969) of the currents and the wind were computed from the low-passed data, and are presented with the simple statistics (means and standard deviations) of the low-passed data of currents, temperature, sea level and wind in Table 1. Since the coast, local isobaths and the principal axis systems of the current meters were aligned very nearly north-south (Figure 1 and Table 1) we did not rotate the coordinate system. The standard deviations of the alongshore (v) and onshore (u) flow decreased with depth, i.e., current fluctuations were strongest near the surface. The strongest mean onshore-offshore flow was at 56 m. The strongest mean alongshore flow was at 81 m. Temperature means and standard deviations decreased with

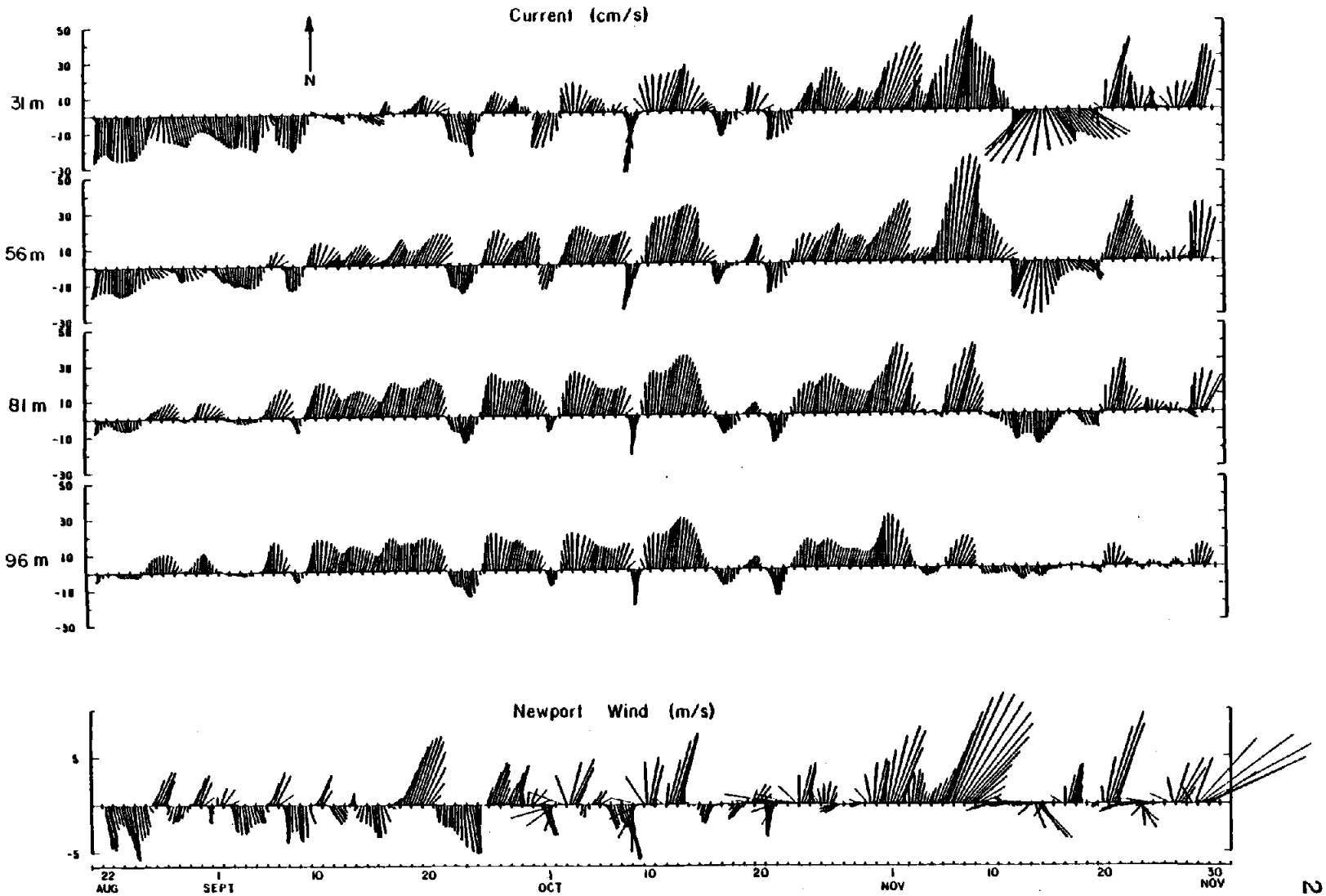

Figure 7. Vector time series of currents and wind.

Table 1. Statistics of the six-hourly low-passed current meter, wind and sea level data. Onshore (u) and alongshore (v) components of velocity, current temperature (T), Newport wind (U and V), wind stress (τ_x and τ_y) and sea level (η): means ($\bar{u}$, $\bar{v}$, $\bar{T}$, $\bar{U}$, $\bar{V}$, $\bar{\tau}_x$, $\bar{\tau}_y$ and $\bar{\eta}$) and standard deviations (u_{SD}, v_{SD}, T_{SD}, U_{SD}, V_{SD}, $\tau_{x_{SD}}$, $\tau_{y_{SD}}$ and η_{SD}).

CURRENT METER DATA

Depth	$\bar{u}$	u_{SD}	$\bar{v}$	v_{SD}	$\bar{T}$	T_{SD}
	(cm/s)				(°C)	
31 m	0.9	5.3	1.6	17.9	9.92	1.79
56 m	1.8	3.7	5.7	15.6	8.89	1.79
81 m	1.3	2.5	7.3	12.7	8.22	0.62
96 m	0.0	1.6	5.9	9.7	8.07	0.51

WIND AND SEA LEVEL DATA AT NEWPORT

	$\bar{U}$	U_{SD}	$\bar{V}$	V_{SD}	$\bar{\tau}_x$	$\tau_{x_{SD}}$	$\bar{\tau}_y$	$\tau_{y_{SD}}$
	(m/s)				(dynes/cm^2)			
WIND	0.0	2.1	0.6	3.2	0.05	0.30	0.10	0.40

	$\bar{\eta}$	η_{SD}
Sea Level (cm)	292.3	6.8

depth. Mean sea level (292.3 cm) during the experiment is within 0.3 cm of the eleven-year mean recorded at Newport (Pittock et al., 1982). The direction of the mean wind was due north (0°T); direction of the mean wind stress was northeastward (26.6°T).

Time series of low-passed alongshore current velocities and temperatures at TURTLE along with wind and sea level from Newport are shown in Figure 8. Visual inspection of this figure shows obvious similarities in the time series of alongshore (v) currents, sea level and northward wind. The seasonal cycle is apparent in the records of temperature, sea level, alongshore currents and the difference of velocity between 31 and 96 m.

Comparisons Between Observations

Correlation coefficients were calculated at lag increments of 6 hours between various linearly detrended low-passed time series (Table 2). The 95% and 99% significance levels were calculated according to Bendat and Piersol (1971, p. 126). Degrees of freedom (integral time scales) were calculated according to Davis (1976). Since the components of the wind correlated better than wind stress with the parameters in Table 2 the wind stress correlations are not presented.

Figure 8. Time series of temperature, alongshore (v) currents and alongshore current difference between 31 and 96 m; sea level and northward (V) wind from Newport.

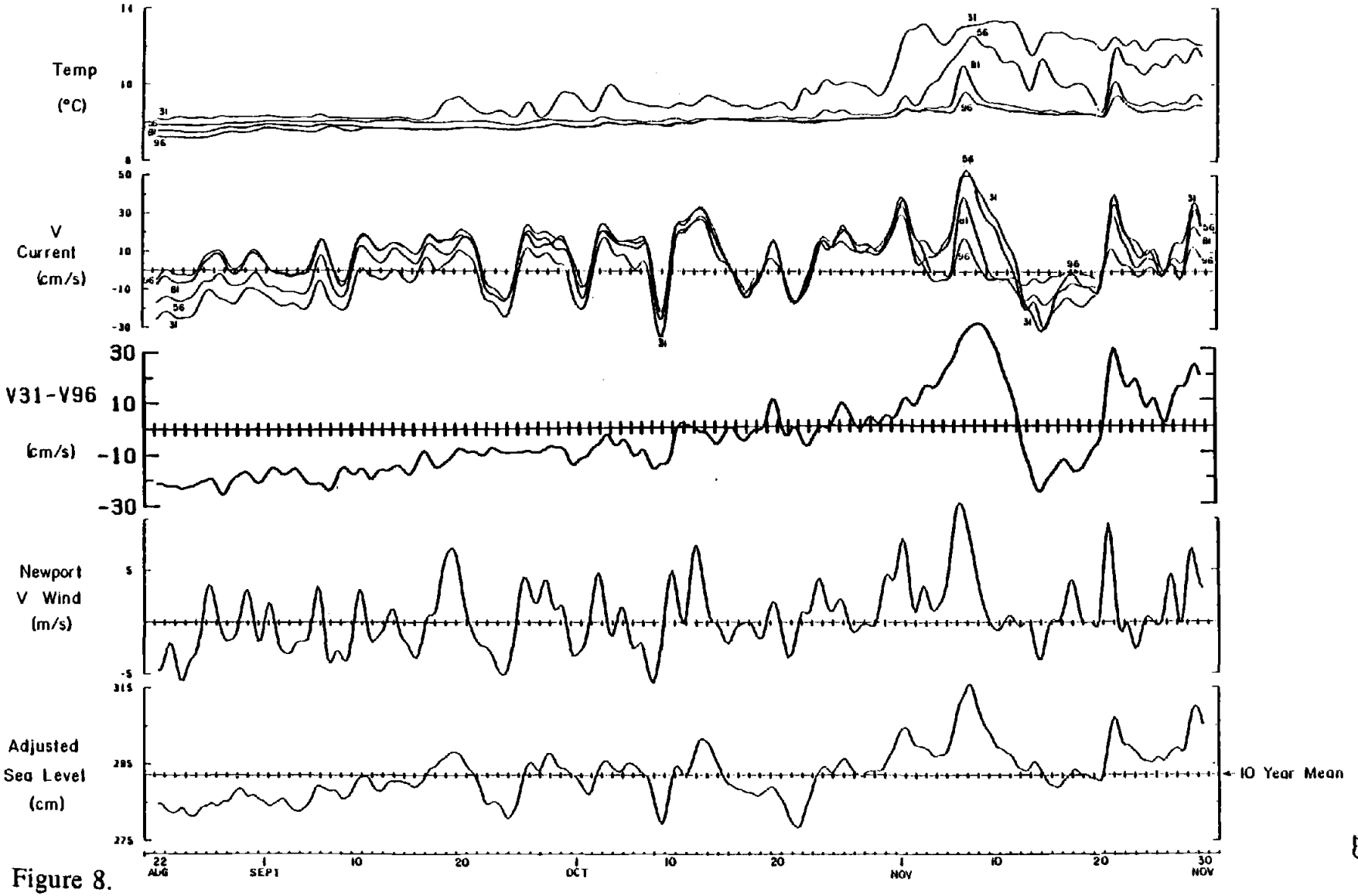
Temp
(°C)
V
Current
(cm/s)
V31-V96
(cm/s)
Newport
V Wind
(m/s)
Adjusted
Sea Level
(cm)
10 Year Mean
22
AUG
1
SEPT
10
20
1
OCT
10
20
1
NOV
10
20
30
NOV

Figure 8.

Table 2. Correlation coefficients between linearly detrended time series (402 six-hourly observations). "CC_m" and "CC_0" are the maximum and zero lag correlation coefficient, respectively. "Lag" is the time in hours of the maximum correlation; positive values of "lag" indicate that the column header leads. "ν" is the degrees of freedom. Correlations are flagged that are below the 95% (•) and 99% (*) significance levels.

	Alongshore Wind				Adjusted Sea Level				Onshore Wind			
	CC_m	CC_0	Lag(hr)	ν	CC_m	CC_0	Lag(hr)	ν	CC_m	CC_0	Lag(hr)	ν
V Current												
31m	0.70	0.54	+(18)	45	0.83		0	29	0.49	0.48	+(6)	50
56m	0.71	0.54	+(18)	50	0.83		+(0,6)	34	0.51		+(0,6)	50
81m	0.72	0.56	+(12,18)	45	0.79		0	31	0.48		0	50
96m	0.67	0.53	+(12)	50	0.68		0	29	0.39		0	50
Sea level	0.75	0.62	+(12,18)	40					0.64		0	50
V_{31}-V_{96}	0.43	0.30*	+(18,24)	50	0.60	0.59	+(6,12)	29	0.43	0.35*	+(18)	50
U Current												
31m	0.28*	0.14•	+(24,30,36)	67	0.17•	0.14•	+(12)	67	0.21•	0.09•	+(30)	80
56m	0.59	0.23•	+(24)	57	0.53	0.49	+(6,12)	40	0.32	0.19•	+(18)	67
81m	0.66	0.18•	+(24,30)	57	0.68	0.58	+(12)	40	0.57	0.40	+(12,18)	57
96m	0.53	−0.17•	+(30,36)	57	0.49	0.25*	+(24)	67	0.37	0.17•	+(18)	80
Temperature												
31m	0.13•	0.08•	+(18,24,30)	50	0.20•	0.19•	+(6,12)	29	0.07•	0.06•	+(6)	57
56m	0.16•	0.07•	+(18,24)	57	0.32•	0.30•	+(6,12)	31	0.24•	0.21•	+(6)	57
81m	0.38	0.25•	+(18)	57	0.47	0.47	+(0,6)	37	0.34	0.32	+(6)	80
96m	0.53	0.25*	+(24)	67	0.63	0.58	+(12)	40	0.38	0.32	+(12,18)	67

General impressions from Table 2 are that onshore winds did not correlate strongly with other time series; alongshore wind correlated significantly with (and led) most of the parameters; and adjusted sea level correlated strongly with alongshore currents at all depths and with current shear. Highest correlations were between adjusted sea level and alongshore current at 31 and 56 m, below 56 m the correlation dropped. Sea level versus alongshore current correlation coefficients were maximum at zero lag, as expected for geostrophically balanced alongshore currents. Alongshore wind correlated highly with alongshore current with currents lagging the wind by 12-18 hours. The alongshore vertical shear, represented by the current difference between 31 and 96 m, correlated better with adjusted sea level than with either wind component. Onshore currents (except at 31 m) were moderately correlated with alongshore wind and adjusted sea level.

Empirical Orthogonal Functions

A complex vector Empirical Orthogonal Function (EOF) analysis was performed on the four times series of current velocity vector observations at 31, 56, 81 and 96 m. In most regards, the technique is similar to scalar EOF analysis with only minor modification needed to generalize it for vectors (Kundu and Allen, 1976). Since it is the fluctuations that are of interest here the data have been demeaned. In this case, up to four real eigenvalues can be generated from the complex covariance matrix of the current velocity observations. Each eigenvalue has an associated orthogonal eigenvector, and the eigenvectors are ordered by decreasing eigenvalue size (amount of energy). The eigenvectors were normalized, such that the sum of the squares of each eigenvector's components is one. Each eigenvector is modified by a complex amplitude time series (same length as original time series) which are uncorrelated at zero lag. The complex time series, C(t), can be represented by an amplitude and phase:

$$C(t) = u(t) + iv(t), \text{ then}$$
$$\text{phase} = \tan^{-1}(\text{imag } C/\text{real } C) \quad \text{and}$$
$$\text{amplitude} = \sqrt{\text{real } C^2 + \text{imag } C^2}$$

It is permissible to rotate the eigenvectors by any arbitrary angle, if the phase time series are rotated an equal angle in the opposite direction. We have arbitrarily chosen to rotate the eigenvectors to the mean phase angle of their corresponding phase's time series. In this way, the time series of phase will fluctuate around zero.

The first and second modes together account for 97.9% of the total energy contained in the original time series. The two other eigenvectors contain only 2.1% of the total energy and are therefore not considered physically important.

The first mode eigenvector accounts for 86.9% of the variance (Figure 9). The components of the first mode form a quasi-barotropic mode, i.e., with upper current components being stronger than deeper current components. All four components of the first eigenvector are directed within seven degrees of each other and there is considerable depth

dependence in their magnitudes: the component at 31 m is 2.5 times greater than the 96 m component. The first eigenvector resembles a surface Ekman layer on top of a bottom Ekman layer: the clockwise veering between 31 and 56 m is consistent with surface Ekman theory and the counterclockwise veering between 56 and 96 m is consistent with bottom Ekman theory.

The second mode accounts for 11.0% of the variance and is a baroclinic mode. The direction of the shallowest component is opposite to the two deepest components (Figure 9).

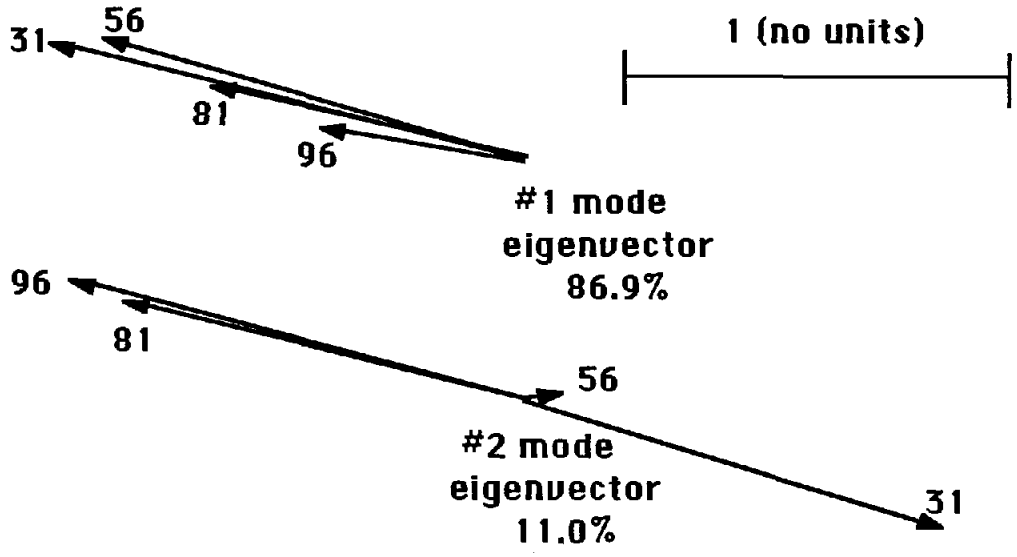

Figure 9. First and second mode eigenvectors.

Figure 10 shows the amplitude and phase time series that modify the first two eigenvectors. An interesting feature of the first mode's amplitude is that during the first half of the time series the peaks are usually associated with positive phase (~90°) and southward current fluctuations, while the troughs are associated with negative phase (~-90°) and northward current fluctuations; during the second half, i.e., after 10 October, peaks of the amplitude time series occur during both positive and negative phase.

The second amplitude time series modifying the baroclinic eigenvector contains much less energy than the first amplitude time series. The peaks are duller and usually occur in conjunction with northward fluctuations, especially during the first half of the time series. The phase of the second mode is bimodal, values during the first half of the time series were typically -90° and during the second half were most often 90°. The largest peak of the second mode's amplitude time series is in early November and occurs during the northward current fluctuation associated with the establishment of the winter regime: this will be discussed further in the next chapter.

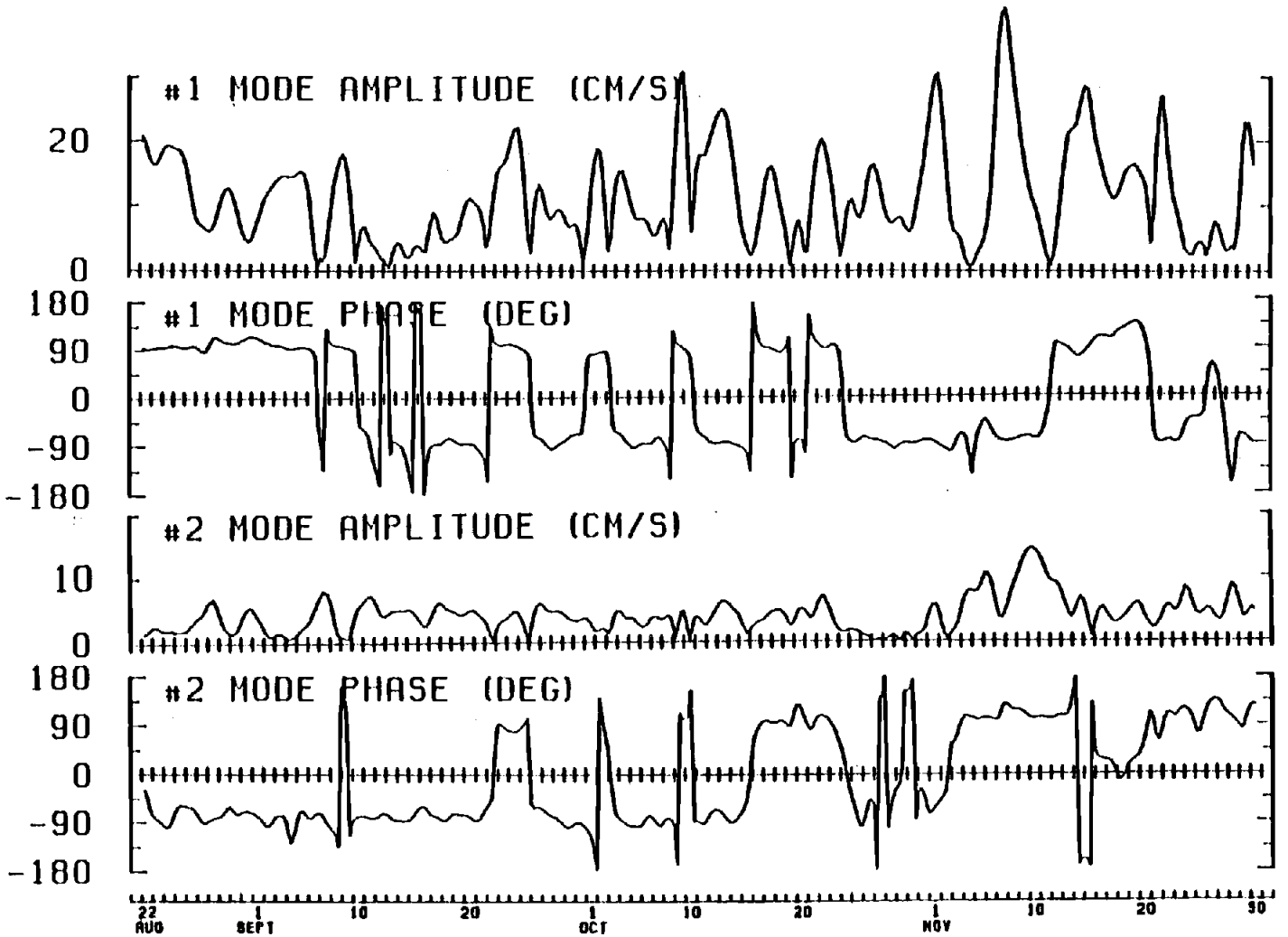

Figure 10. Amplitudes and phases for the first and second mode eigenvectors. Positive phase rotates the eigenvector counterclockwise and negative phase rotates the eigenvector clockwise.

III. THE FALL TRANSITION

Relationships between hydrographic, current meter, wind and sea level data are used to describe the basic characteristics of the autumnal oceanographic transition. It is first shown in this chapter that the summer regime was still present in Oregon coastal waters when the experiment began on 21 August and that it persisted until 10 September. Next shown is the establishment of the winter regime during 11 days of continuous northward wind stress in early November. Finally, the transitional period between the summer and the winter regimes is examined: the south to north reversal of near-surface currents, the leveling of the frontal layer, the shoaling of the poleward undercurrent and changes of alongshore current shear.

The Observed Summer Regime, 1980

A good example of an upwelling regime is exhibited in the sigma-theta distribution calculated from the CTD section made on 21 August (Figure 5). The seasonal pycnocline (24.5 to 25.0 isopycnals) broke the surface about 7 km offshore. The deeper permanent pycnocline (between the 25.5 and 26.0 isopycnals) tilted upwards towards the coast

and came within 9 m of the surface 3 km offshore: the 25.5 isopycnal was level at a depth of 60 m from 95 to 45 km offshore, where it began to rise steeply towards the coast; the 26.0 isopycnal was level at a depth of 100 m from 95 to 45 km offshore, from 45 km it began sharply rising and converging with the shallower 25.5 isopycnal. A hydrographic section on 26-27 August 1972 (Smith, 1974, Figure 3) within 25 km of the coast shows essentially the same profile as the August 1980 section. Collins (1964, Figure 5) exhibits a July 1972 sigma-t section and termed it a "classic" upwelling profile. Comparing that section to the 21 August 1980 section shows the frontal layer during July was about 20 m shallower at 94 km offshore, 30 m shallower at 50 km from shore and broke the surface 19 km from shore where the frontal layer during 21 August was about 40 m deep. In summary, the frontal layer is shallower and more steeply inclined during "classic" or strong upwelling than it was on 21 August 1980.

Also evident in the August 1980 section is the Columbia River plume, between 5 and 35 km offshore, with its low salinity water (<32‰) swept southward by the prevailing southward currents (Figure 4).

Calculations of dynamic height along selected pressure surfaces show strong baroclinicity within 35 km of the coast where upwelling was most intense (Figure 5). In this region, isobars above 100 meters

descended rapidly towards the coast, but below 150 meters they were essentially flat. The sea surface isobar relative to 500 db, level between 95 and 35 km offshore, dipped sharply from 35 km towards the coast by about 15 dyn cm. Huyer (1977) found that across the Newport line the mean of the sea surface isobar relative to 600 db taken from several sections during the month of August dropped about 6 dyn cm from 35 km to the coast, and dropped another 6 dyn cm between 35 and 83 km offshore.

Initial observations at current meter mooring TURTLE confirm that the summer regime was still present during late August and early September (Figures 7 and 8): the near-surface current at 31 m was steadily southward (even during northward wind events) until 10 September. Near-bottom currents at 81 and 96 m were more coherent than the shallower currents with wind fluctuations during the first month of observations: northward and southward winds were associated with northward and southward near-bottom currents, respectively (Figure 11). Mean currents were very baroclinic with deeper flow more poleward, showing another characteristic of the summer regime: the poleward undercurrent (Smith, 1974; Huyer et al., 1976; and Halpern et al., 1978). Current fluctuations were barotropic; these depth-independent fluctuations have been previously observed during summer by Smith (1974) and Huyer

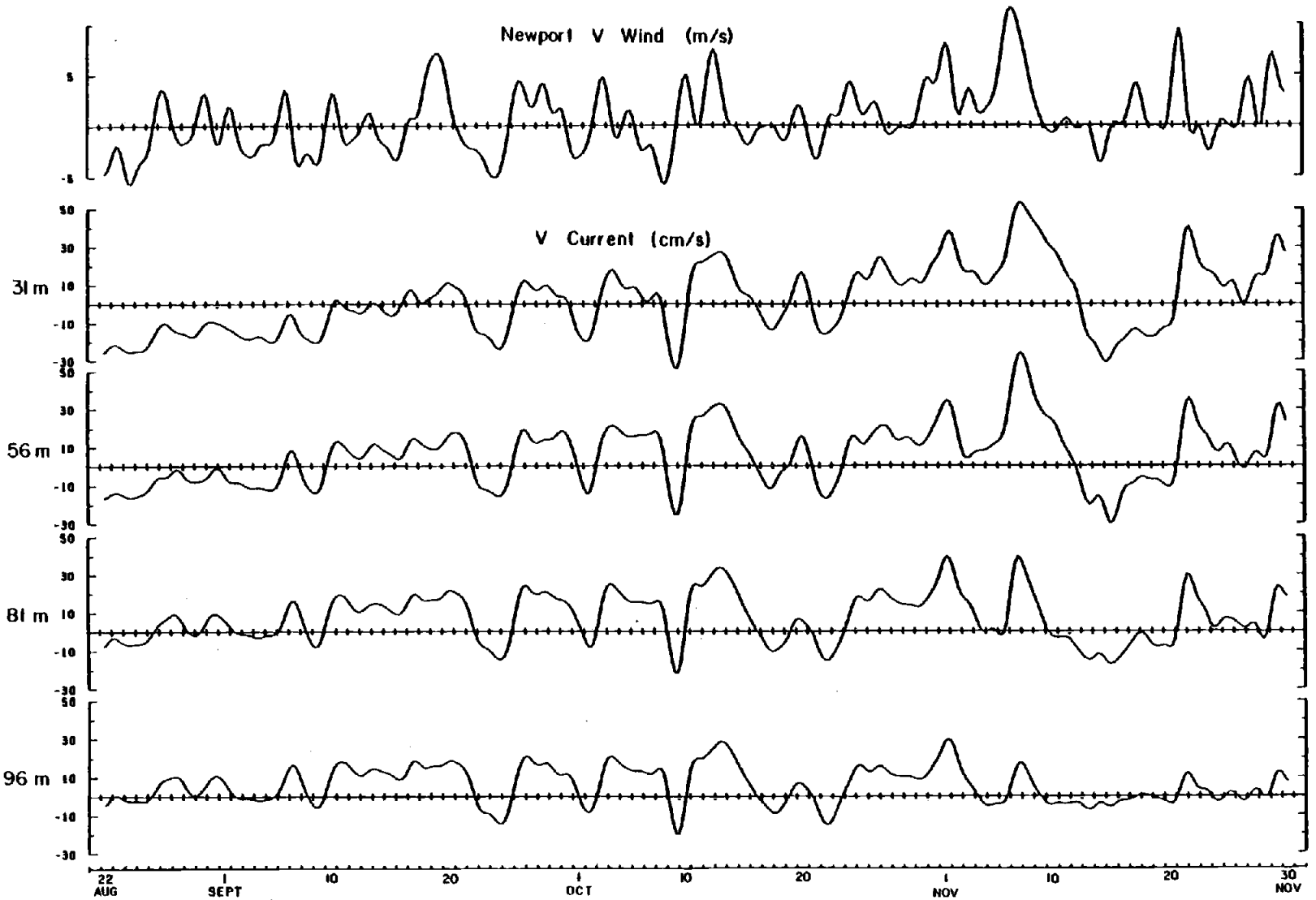

Figure 11. Time series of northward wind and alongshore currents.

et al., (1978). The velocity difference between 31 and 96 m (Figure 8), had values ranging between -20 and -25 cm/s, typical of late summer (Huyer et al., 1979; Sobey, 1977, Figure 6). Water temperature (Figure 8), measured by temperature sensors at the mooring, was cold (<8.5° C) at all depths until 18 September, indicating the presence of upwelled water; the seasonal thermocline formed by surface heating and the Columbia River plume was above the shallowest current meter (Figure 4).

Parallel observations of winds and sea level at Newport were also characteristic of late summer in Oregon. Sea level's ten-year mean during August is 285.2 cm (Pittock et al., 1982); during the first week of observations sea level was very close to this value (Figure 8). Mean winds of late summer (from 22 August to 10 September) were southward with frequent short duration northward events (Figures 7 and 8).

The ending of the summer regime and the beginning of the transitional period is marked by trends of several different parameters on 11 September. Sea level, near-surface currents, the bottom boundary layer, alongshore current shear and the poleward undercurrent began exhibiting characteristics that were different from typical summer conditions on 11 September. The beginning of winter conditions is examined in the next section of this chapter and the remainder of the

chapter examines the transitional period.

The Onset of the Winter Regime, 1980

During the first week of November, two strong northward wind events punctuated eleven days of continuous northward winds, from 30 October through 9 November (Figures 8 and 11). These two events were stronger than any preceding winds: the first event peaked on 1 November with velocities greater than 8.5 m/s and the second event peaked on 7 November greater than 12.5 m/s (Figure 7). Strong northward winds are common during late fall and winter off Oregon as the Aleutian Low pressure system strengthens and storms break off and move eastward over the continental U.S.

The ocean's response to the strong northward winds resembles a surface Ekman layer, i.e., with onshore surface flow. Currents at 31 and 56 m were almost continuously strong and onshore during this period (Figure 12). Large near-surface onshore currents advect warmer surface water downwards (and, in this case, the permanent pycnocline); this is reflected in the temperature time series at the mooring (Figure 8). Temperature rose dramatically, at 31 m on 31 October, at 56 m on 3 November and at 81 and 96 m on 6 November.

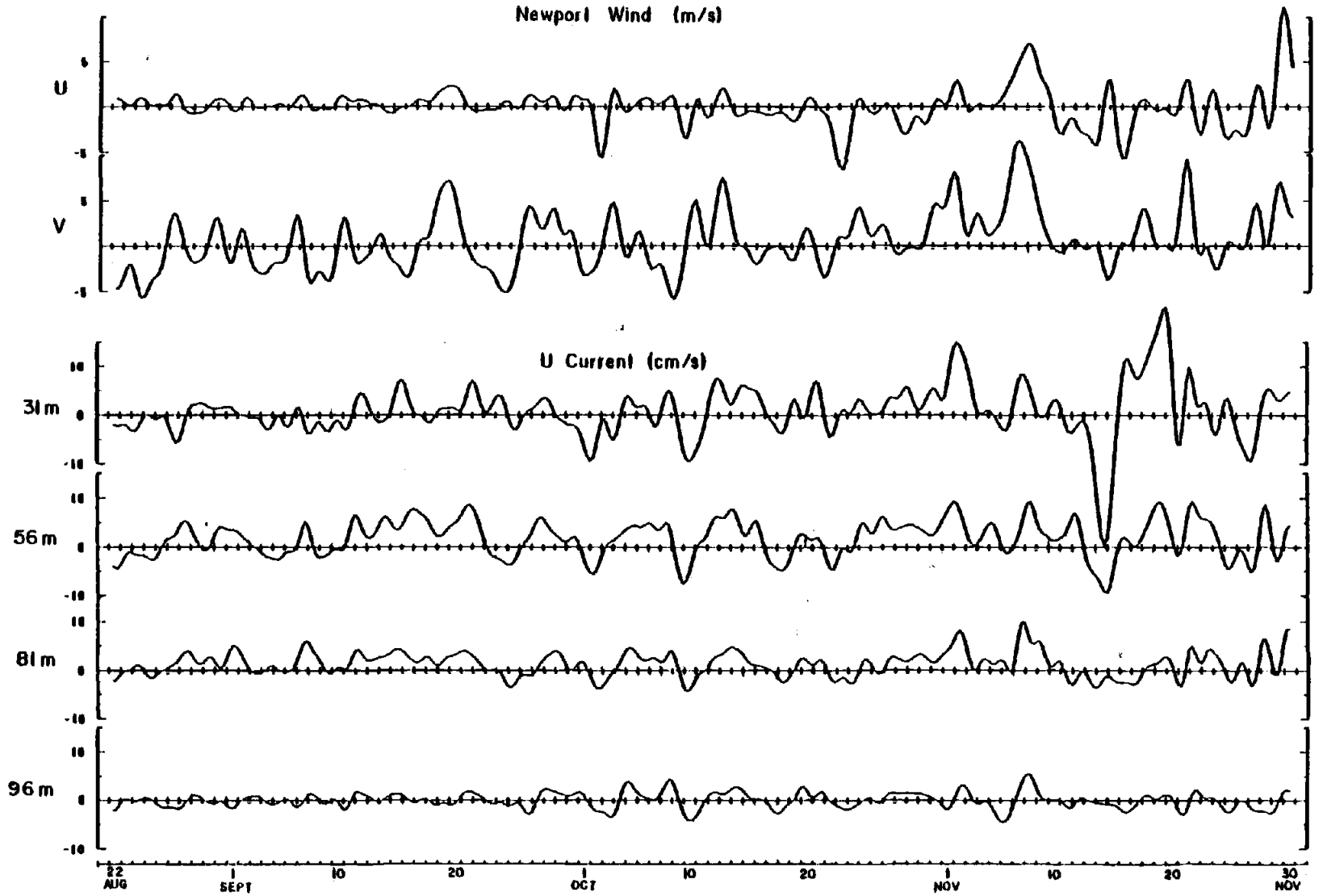

Figure 12. Time series of onshore (u) currents and eastward (U) and northward (V) winds.

Each of the five hydrographic sections were taken approximately monthly. It should be pointed out that temporal aliasing of hydrographic data may occur due to the quick response (on the order of one day) of the ocean to wind stress fluctuations; nevertheless, Figure 13 gives a good snapshot of the permanent pycnocline before and after the long period of northward winds. The permanent pycnocline (approximated by the 25.75 isopycnal in Figure 13) on 30 October was 50 m deep and slightly inclined; on 18 November, it was 80 m deep and level. A pycnocline depth of approximately 80 m is typically observed over the shelf during winter (Collins 1964, Huyer, 1977; Huyer et al., 1979).

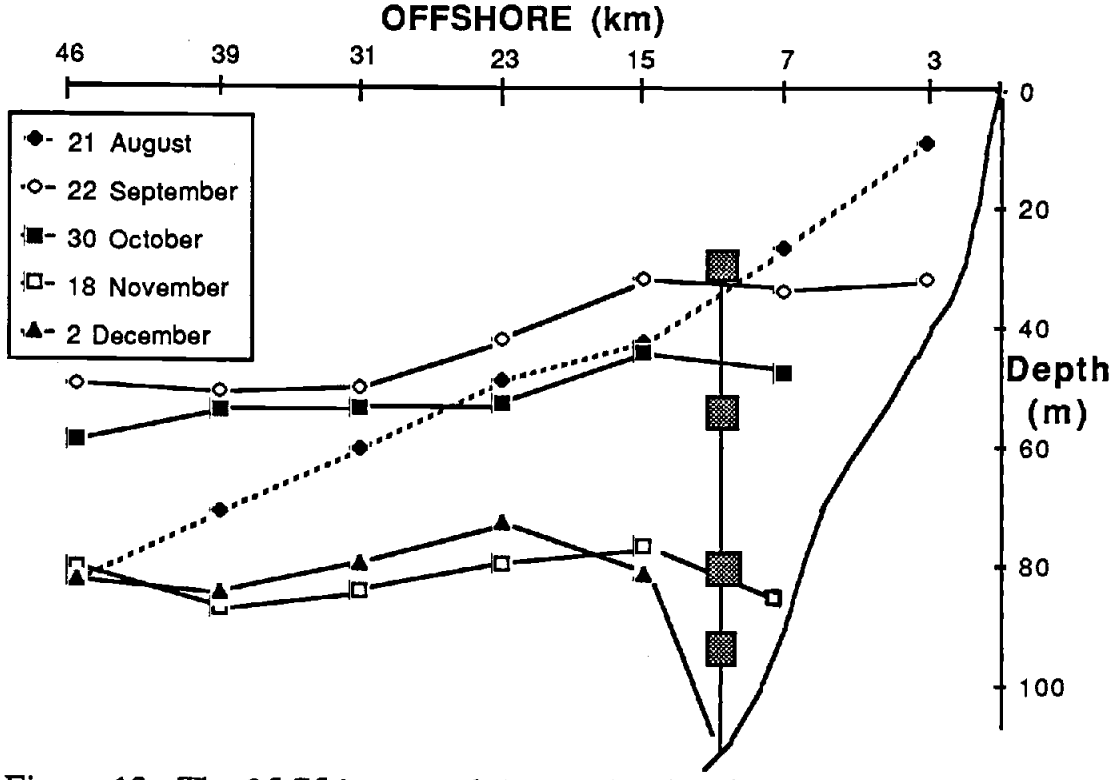

Figure 13. The 25.75 isopycnal during the five CTD sections.

Coastal sea level responded to the northward wind events of early November by rising from its minimum value of the data record (278.1 cm) on 22 October to its maximum (316.1 cm) on 9 November (Figure 8). The current difference between 31 and 96 meters, close to zero during late October, also rose sharply in early November and began a series of strong wind-driven fluctuations (Figure 8). Sea level subsequently stayed high (although dipping slightly below the long-term mean during southward winds on 16 and 20 November) until the end of the data record on 30 November. Sea level's long-time mean during November (298.2 cm) (Pittock et al, 1982) is extremely close to mean value (298.9 cm) of sea level during the period that extends from the beginning of the winter regime (on 7 November) through the end of the data record. High sea level (Reid and Mantyla, 1976; Marthaler, 1977; Huyer et al., 1978) and strong fluctuating shear (Huyer et al., 1978) are features of the winter regime.

Alongshore current fluctuations after these wind events were baroclinic (Figures 7 and 8). Mean flow during the winter regime of 1980 showed deeper currents weaker than surface currents regardless of current direction. There were occasions when near-bottom current was weakly equatorward while currents in the rest of the water column were poleward, e.g., on 4-6, 24, 26 and 28 November.

NOAA northern hemisphere six-hourly weather maps (not shown) show that the northward wind events (Figures 8 and 11) that occurred before 20 September were caused by small low-pressure systems or fronts with a synoptic scale of ~500 km. The later and stronger northward wind events of fall were much larger scale, ~3000 km, extending from northern California to Alaska. The reader is directed to Anderson et al. (1983) for a weather map of a typical large scale fall low-pressure system.

The Transition Period

The beginning of the transitional period is on 11 September. As mentioned earlier, the beginning of the transition is apparent in several different parameters, e.g., alongshore current shear, sea level, near-surface currents, the bottom boundary layer and the poleward undercurrent. This chapter and the next describes the different behavior of these parameters during the fall transition.

The Decay of Southward Surface Currents During Autumn

Southward near-surface current did ***not*** disappear as a result of a single strong wind stress event. Before 11 September, near-surface currents were always southward (Figures 7 and 14). On 11 September,

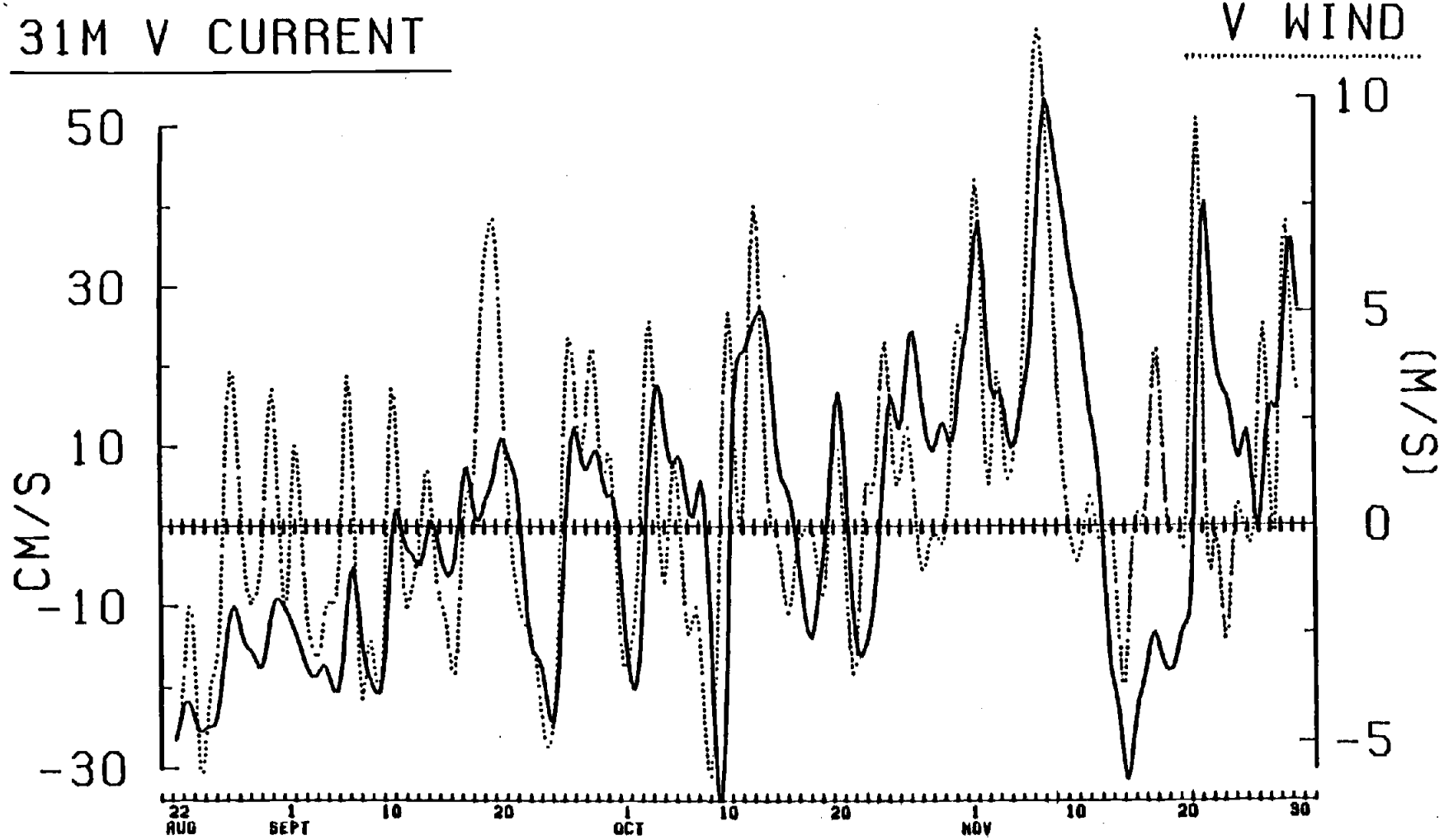

Figure 14. Time series of 31 meter alongshore (v) current and northward (V) wind. The solid line denotes current, measured by the left axis; the dotted line denotes northward wind, measured by the right axis.

near-surface currents were northward and the wind event associated with this current reversal was not dramatic: it was a short and not particularly strong northward wind. Several preceding northward wind events, e.g., 27 and 30 August and 6 September, had been as strong or stronger (but not enough to force northward near-surface current flow).

While northward surface current events of short duration are not uncommon during the summer regime, the southward flow pattern is usually quickly re-established (Smith, 1974). The significance of the 11 September event was that this re-establishment did not occur; although there were southward current events after 11 September, the mean flow was northward. After 11 September all northward wind events forced northward flow (even minor northward wind events, e.g., on 13 September and 20 October).

The 11 September northward wind event, when compared to preceding wind events, forced a strong fluctuation towards positive alongshore current flow. Close examination of Figure 14 shows that beginning in September, northward wind effects on near-surface currents were becoming more apparent than the effects of southward winds; in summer usually the reverse is true (Smith, 1974). There were four comparable northward wind events in late August and early September (27

and 30 August, 6 and 11 September). A progressively stronger northward current fluctuation was associated with each of the last three events. The northward wind event on 6 September produced a stronger northward current fluctuation than the two preceding northward wind events with comparable wind velocities on 27 and 30 August. As mentioned before, even the weak (1 m/s) northward wind event on 13 September forced northward current. Southward wind events often forced strong southward currents greater than 20 cm/s, e.g., on 29 August and 5, 9 and 24 September and 2 and 9 October; chronologically, however, starting from the beginning of observations until 13 October, each successive northward wind event forced a northward current fluctuation that was more poleward than the last (except the small northward event on 13 September).

In summary, there was a combination of effects which was involved with the decay of southward near-surface current: first, in a reversal of a phenomenon observed during summer, the effect of northward winds was stronger than the effect of southward winds on near-surface current; second, early in the data record, the northward wind events, even though comparable in magnitude and duration, were forcing progressively stronger current fluctuations; and third, later northward wind events of fall (e.g., 17-20 and 26-30 September, 10-13 and 22-25 October) often

lasted four or more days. These events were stronger than the earlier northward wind events which usually lasted only one day; this forced the continuing trend of increasing poleward flow.

Why was the minor wind stress event on 11 September sufficient to cause the decay of southward near-surface flow when recent stronger wind events did not produce the same effect? Currents on the Oregon continental shelf have been shown to be in near-geostrophic balance, where northward and southward surface flow over the shelf is balanced by the rising and lowering of sea level at the coastal boundary (Collins, 1968; Smith, 1974; and Huyer et al., 1978). The southward surface currents of late August and early September that persisted during northward winds were geostrophic currents caused by previous offshore transport of water which caused the sea surface to slope downwards towards the coast. Sea level, since it is a measure of the sea surface slope, is an indicator of the direction of near-surface currents over the shelf.

Marthaler (1977) established that alongshore near-surface currents off Oregon could be modeled by regression upon coastal sea level. The regression is reliable because of the high linear correlation coefficient, which measures the degree of association between variables, in this case 0.87. We regressed observations of sea level at Newport on the 31 m

alongshore current at TURTLE. In the regression a sea level value of 291.9 cm was obtained as the zero-intercept on the alongshore current axis, i.e., when sea level is above 291.9 cm, northward current is predicted. It is mentioned that the value obtained from the regression is extremely close to the long-time mean of sea level at Newport, 292.1 cm (Pittock et al., 1982); to the mean of sea level for this experiment, 292.3 (Table 1); and to the mean of sea level for the transitional period between the end of the summer regime and the beginning of the winter regime, 291.1 cm (Table 4). The regression also indicated sea level rising 0.34 cm for each one cm/s rise in current.

The results of the regression can be visually compared to Figure 15, where every zero crossing in the 31 m alongshore current has a synchronized near-simultaneous crossing of sea level past its mean (the one exception occurred during the northward fluctuation on 19-20 October).

It should be mentioned that the intercept of 291.9 cm obtained here was about 5 cm lower than the value obtained by Marthaler. This difference could be partially explained by the different depths of current meters, where Marthaler used current meters between 20 and 25 m, while in this study a depth of 31 m was used. Sea level regressed on current observations at shallower depths will result in a higher intercept value (in a

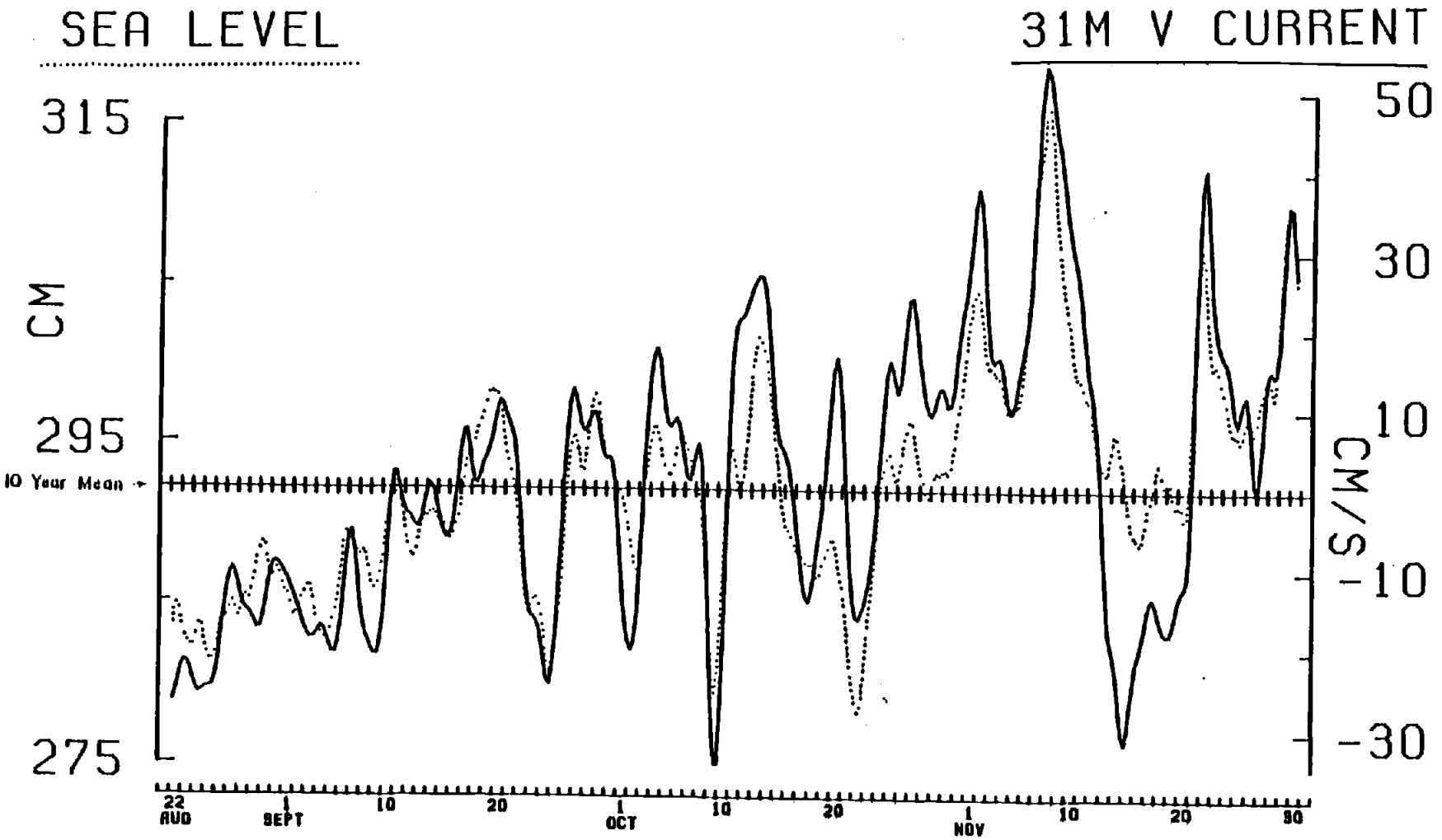

Figure 15. Time series of 31 meter alongshore (v) current and Newport sea level. The solid line denotes current, measured by the right axis; the dotted line denotes sea level, measured by the left axis.

region of alongshore current shear, $\partial v/\partial z < 0$).

The Shoaling of the Poleward Undercurrent

The vertical structure of alongshore currents is shown in Figure 16 by calculations of ten-day means of relative alongshore velocity. Relative velocity is calculated by subtracting the ten-day mean of near-bottom current (96 m) from means at each depth: as a result of this calculation the bottom value will be zero. Since the slope of relative velocity between current meters is proportional to shear, one can clearly judge the sign, vertical position and strength of current shear.

During the first ten-day average between 22-31 August, relative alongshore current was poleward with depth; i.e., the poleward undercurrent was strongest at the deepest current meter. The next ten-day mean, 1-10 September, was similar to the previous mean between 31 and 81 m, but between 81 and 96 m, velocity difference decreased. After 10 September, relative velocity between 81 and 96 m reversed sign, with current at 81 m the most poleward: this is interpreted as a shoaling of the poleward undercurrent. The next several ten-day means reflect further surfacing of the poleward undercurrent with relative velocity gradually

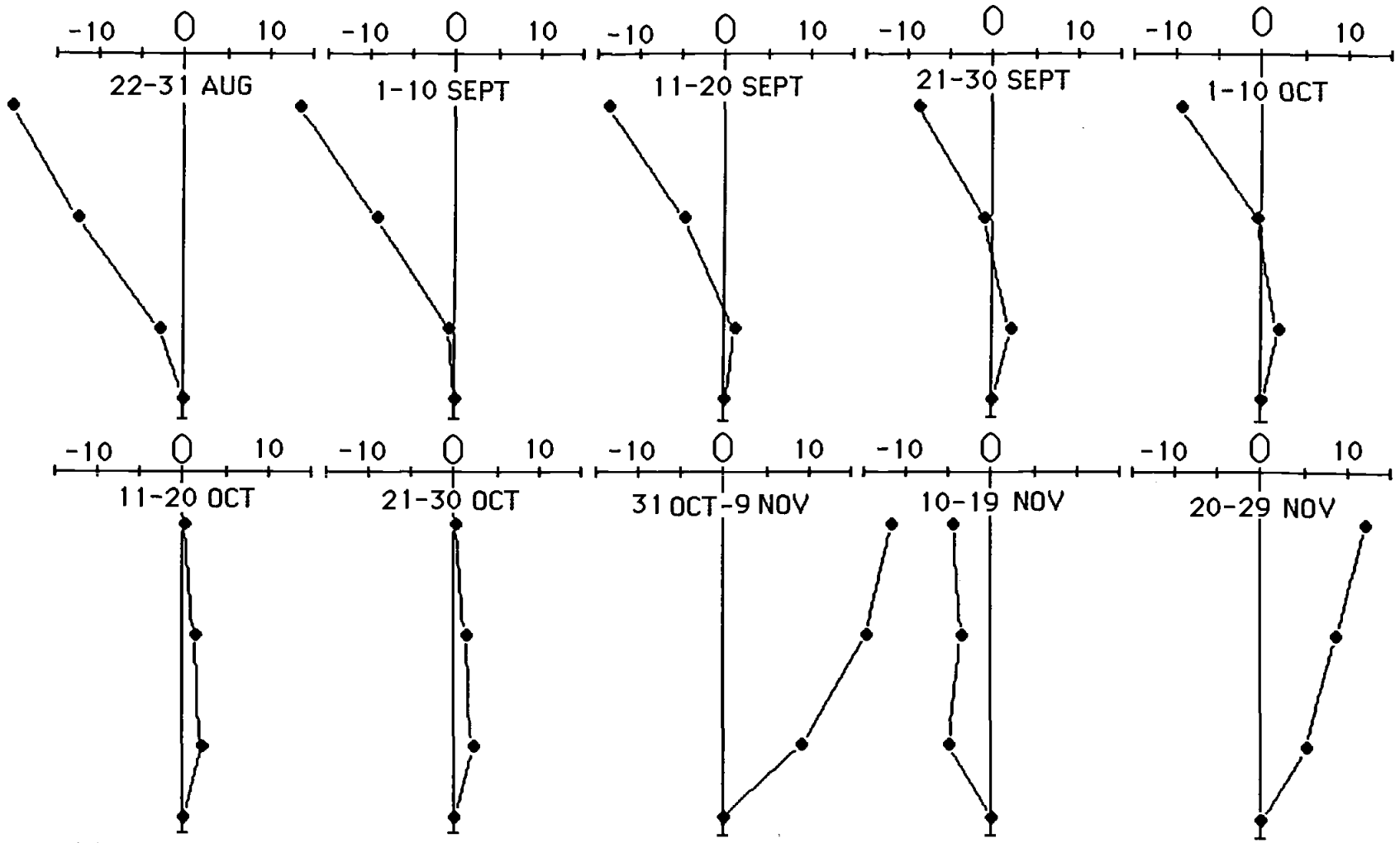

Figure 16. Ten-day means of relative alongshore current velocity difference. Calculated by subtracting the mean at 96 meters from the mean current at all depths.

decreasing between 81 and 56 m. Between 11-30 October, the two ten-day means exhibit a barotropic field: relative velocity between 56 and 31 m, remarkably constant heretofore, disappeared. After 30 October, the last three ten-day means fluctuated strongly from positive to negative.

Figure 17 clearly illustrates the shoaling of poleward current in approximately monthly means calculated in the same manner as Figure 16. The first mean shows the deepest current meter recorded the strongest poleward current; the second mean shows the strongest poleward current at 81 m; the third mean has poleward current slightly stronger at 56 m; and the last mean shows poleward current strongest at 31 m.

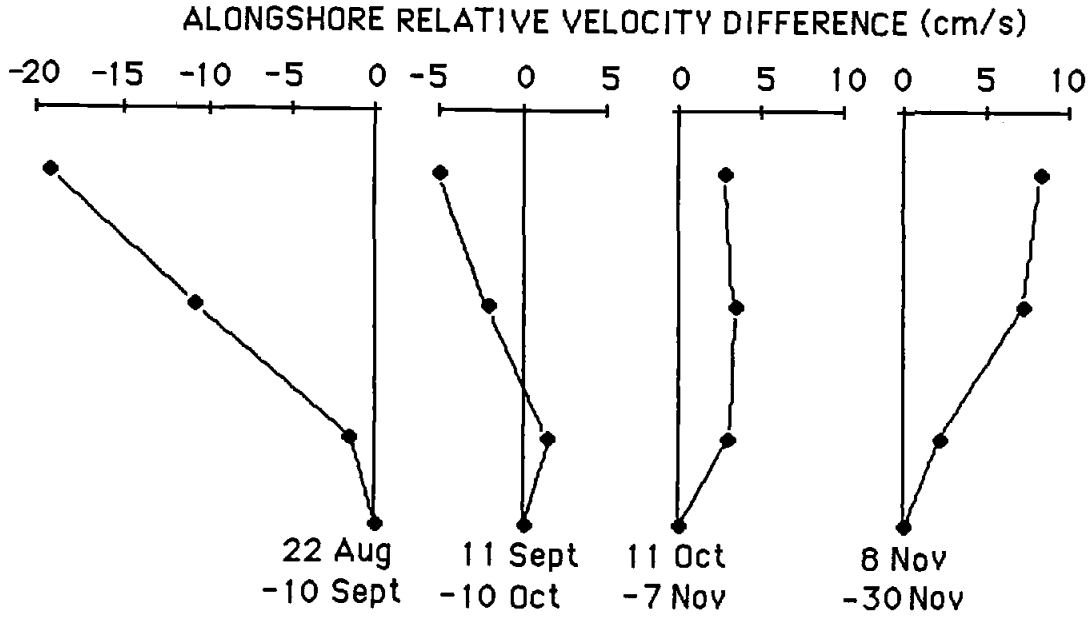

Figure 17. Variations of approximately monthly means of relative velocity difference with depth: 31, 56, 81 and 96 m.

In order to examine in detail the gradual rising of poleward current, Figure 18 shows time series of alongshore current shear between adjacent current meters and between the shallowest and deepest current meter. Current shear ($\partial v/\partial z$) is calculated by dividing velocity difference (∂v) at two different depths by the vertical separation (∂z): $\partial v/\partial z=(v_1-v_2)/(z_1-z_2)$, giving units of s^{-1}.

Shear between the near-surface and near-bottom current meters, at 31 and 96 m, exhibited a long, gradual trend towards positive values, from 22 August until early November. After early November, shear fluctuated strongly between positive and negative: a signature of the winter regime (Huyer et al., 1978).

Shear between the deepest current meters, 81 and 96 m, was initially negative, but by 11 September was more often positive, i.e., positive values indicating the poleward undercurrent was stronger at 81 m.

Shear between the intermediate depths, 56 and 81 m, stayed fairly constant until 11 September. Then, following the pattern established between the two bottom current meters, the shear began slowly decreasing. The first change to positive values occurred during late September. During the month of October, there were many events when the current at

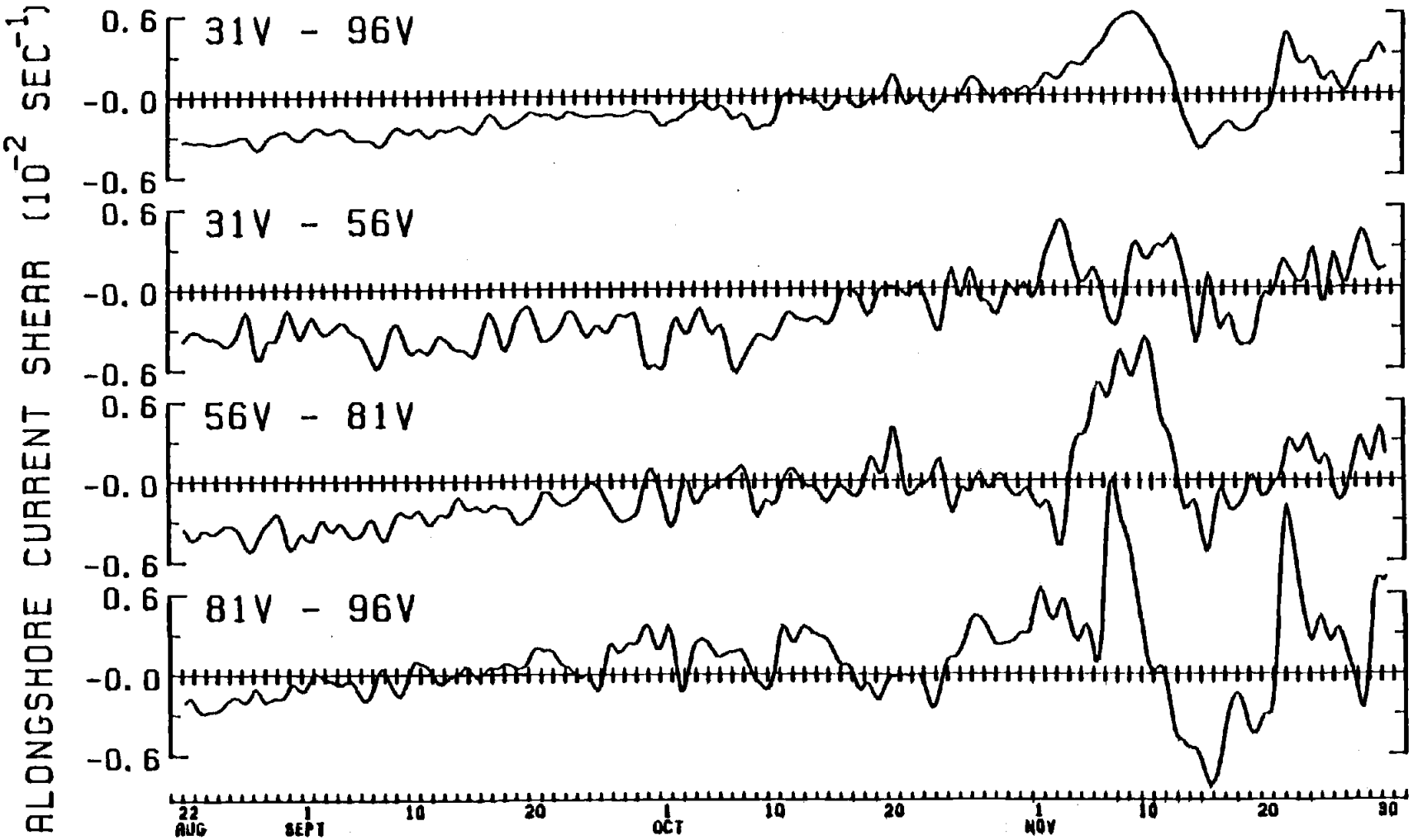

Figure 18. Time series of current shear between the shallowest and deepest current meters: 31-96 m; and between adjacent current meters: 31-56 m, 56-81 m and 81-96 m.

56 m was more poleward than current below at 81 m and above at 31 m, e.g., on 1, 3, 7, 11, 18-20, 24, and 29 October: clearly the signature of the vertical ascension of poleward currents induced by density effects.

Shear between the shallowest current meters, 31 and 56 m, was not positive until 20 October. The positive shear that occurs after late October was probably due to northward winds, which had stronger effects on currents closer to the surface.

Were rising poleward currents during fall implicated with the decay of southward surface currents as speculated in the INTRODUCTION? Earlier we have shown the transition of surface currents began on 11 September. By that date, the strongest poleward current had risen to 81 m. Not until 29 September had the strongest poleward current risen to 56 m. It seems clear that the rise of the poleward undercurrent did not replace southward surface currents with poleward flow.

The Transition in the Density and Temperature Field

The long time scale and gradual trend of decreasing current shear during the transitional period leads one to expect there was similarly slow leveling of the steeply inclined frontal layer observed over the shelf on 21

August. Figure 19, which shows frontal profiles for the five different hydrographic sections, is consistent with this hypothesis.

The 21 August frontal layer rose strongly from 46 km to close to the surface a few km offshore. A gentler tilt, uniformly extending 125 km offshore, was observed one month later on 22 September. The frontal profile on 29-30 October remained weakly inclined, although winds during the previous five days were northward. The sections on 18 November and on 2 December were made after the slow trend in current shear ended: there was no remainder of a tilted frontal layer over the shelf, although further offshore of 62 km the frontal layer remained inclined.

Each of the five sections were taken approximately one month apart and no hydrographic data is available between the sections, but qualitatively, the notion of a slow transition in the offshore density field is supported by the gradual lessening of frontal layer tilt observed in the first four sections (Figure 19).

Time series of temperature at the mooring (Figure 20) mirror the deepening of the frontal layer seen in Figure 19. At the beginning of the record, temperature at all depths were cold. The hydrographic section on 21 August shows the seasonal thermocline was above the shallowest current meter (Figure 4). The temperature time series show little variation during

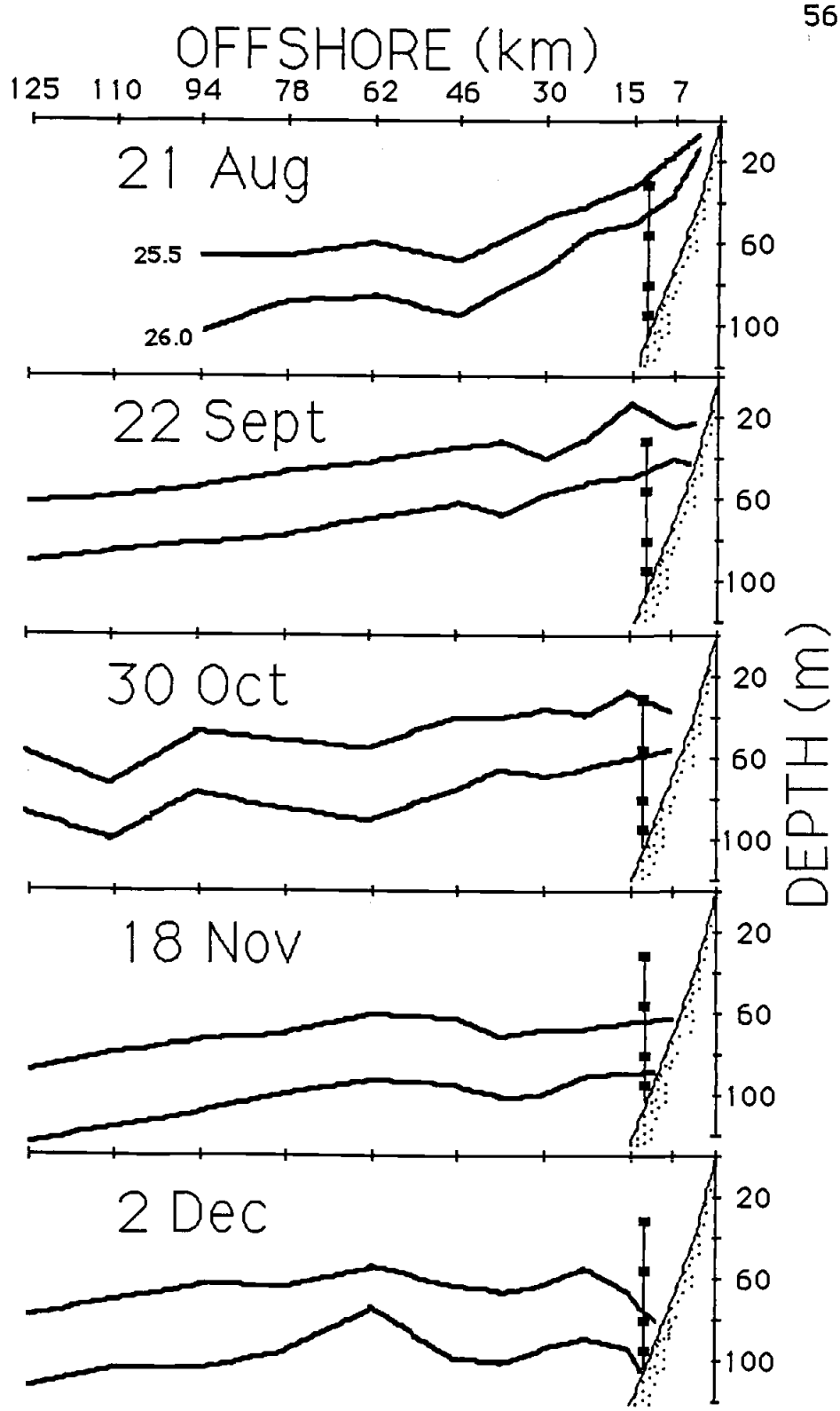

Figure 19. The frontal layer (25.5 and 26.0 isopycnals) during the five different hydrographic sections.

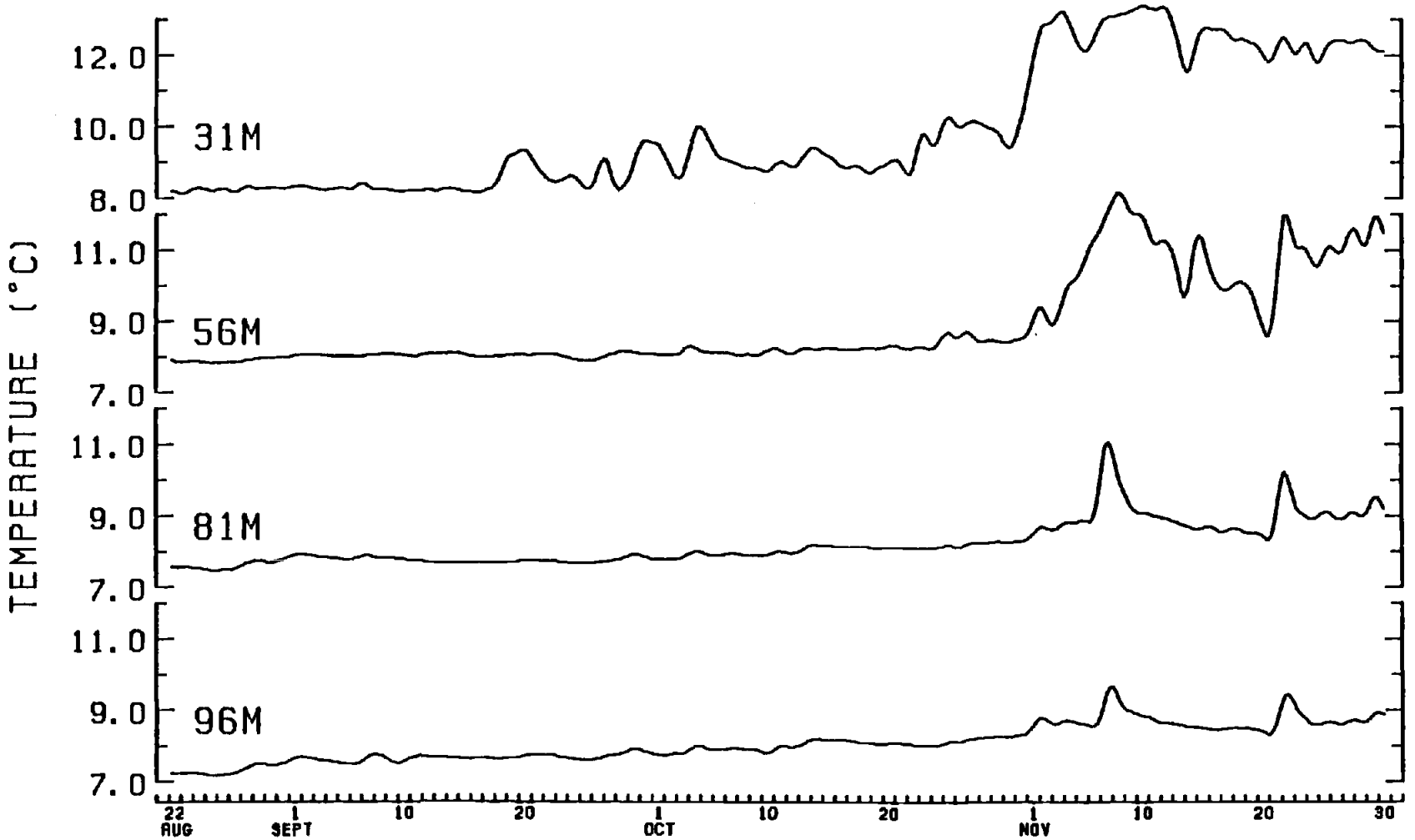

Figure 20. Time series of temperature from the current meter mooring.

the first month of the record with temperature at all depths staying below 8.5° C. During the northward wind event on 20 September, the thermocline (or the upper portion of the pycnocline) was lowered to the depth of the temperature sensors at 31 m and temperature rose ~1°. Thereafter, fluctuating temperature at 31 m between 20 September and late October was a wind-driven response to northward and southward winds which lowered and raised the pycnocline, respectively. The strong northward wind events in early November lowered the pycnocline in the water column, abruptly affecting temperature first at 31 m, and shortly later at 56, 81 and finally 96 m. In an earlier section describing the observed winter regime, it has been shown that this event marked the beginning of winter conditions; which is also to say it marked the end of the transitional period.

Discussion

The fall transition was gradual and lasted approximately two months. The shorter spring transition, occurring in one week or less, is apparently on the "event" time scale. The fall transition is clearly much different from the spring transition. The fall transition's asymmetry with the spring transition suggests different dynamical mechanisms. And due to

the longer time scale the question is raised whether the fall transition is really a transition, or whether it is a separate oceanic season that is as different from the winter and summer regimes as those two regimes are to each other. Or is the transition merely a form of slow "blending": gradually relaxing summer conditions converging with winter conditions slowly strengthening?

The Transition of Alongshore Currents

Differences in the alongshore current field from typical summer conditions appeared first at the lowest depths (Figure 21). By 11 September, the strongest poleward current was at 81 m. Currents at 56, 81 and 96 m evolved gradually into a barotropic field after 11 September, i.e., by slowly possessing similar values. Baroclinic effects were confined between 31 and 56 m, until the strong current fluctuation on 8-10 October, when the entire water column became barotropic; near-surface current at 31 m, which was always more southward than deeper currents, was equal to deeper currents.

Current fluctuations were summer-like, i.e., barotropic during the entire transitional period. Barotropic current fluctuations lasted until early November, the beginning of the winter regime. With the onset of

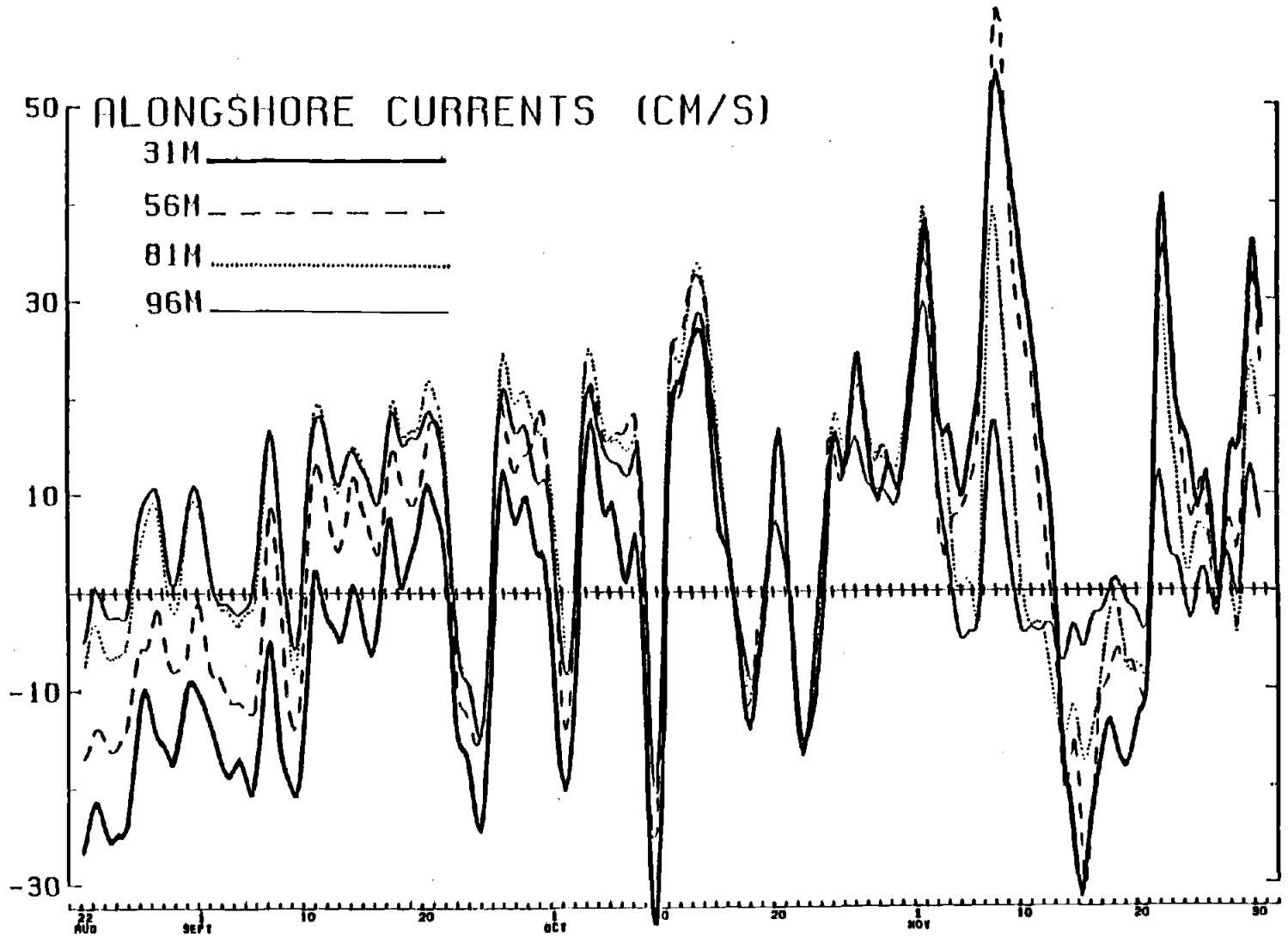

Figure 21. Time series of alongshore currents.

winter conditions, alongshore current fluctuations became baroclinic with deeper current weaker than surface current regardless of current direction.

In summer, mean currents are often observed with a zero crossing in the water column (Halpern et al., 1978); after the wind fluctuation on 20 September, currents were always the same sign, although there was still considerable shear present. Current fluctuations changed sign within a day of each other and often seemed to change sign simultaneously, e.g., on 26 September, 3, 16, 19, 21 and 24 October.

In "winter" the strongest flow usually occurred at 31 m, regardless of current direction. During the "fall", the strongest flow occurred at 31 m only during southward fluctuations, as is the case during "summer". During early "fall", the strongest flow during northward fluctuations was at 81 meters; during late "fall" (i.e., after 10 October), the strongest flow during northward fluctuations usually occurred at 31 or 56 meters.

In summary, the transition from the summer regime with a baroclinic mean was achieved by a slow evolution of the water column into a regime with a barotropic mean. First, the lower half of the water column became barotropic, and by mid-October, the entire water column became barotropic. Mean fall currents were northward at all depths as they were

during winter. Fluctuations during the entire transitional period continued to be barotropic as in summer.

The behavior of alongshore currents suggest the transition was not uniquely different from either the summer or winter regime, since components of both regimes were present, i.e., mean northward currents at all depths were winter-like and barotropic fluctuations were summer-like. However, the poleward undercurrents slow ascension in the water column is an anomalous characteristic that has not been observed during different seasons.

IV. THE BOTTOM BOUNDARY LAYER

In the last chapter, the transitional period was described as beginning on 11 September and ending on 6 November. Inspection of the time series from the moored current meters (Figure 8) shows that the temperatures at depths of 81 and 96 m were nearly the same for much of this period. These records suggest that both instruments may have been within an isothermal bottom boundary layer (BBL) through most of the transition period. In this chapter, we investigate the nature of the BBL, by examining time series of temperature difference, by estimating the thickness of the BBL, and by determining whether there is any veering of the current at these depths. Since we are especially concerned with the proximity to the bottom, subscripts in this chapter will denote height above the sea floor rather than depth below the sea surface. The water depth at Turtle was 106 m: thus the current meter at 96 m depth was at 10 m height, the current meter at 81 m depth was at 25 m height, etc.

Figure 22 shows three time series generated from current meter data: (1) the difference of water temperature ($\Delta T=T_{25}-T_{10}$) between 25 m and 10 m; (2) the observed instantaneous angle (θ) of veering between current vectors at 25 and 10 m (plotted only if the current velocity at both

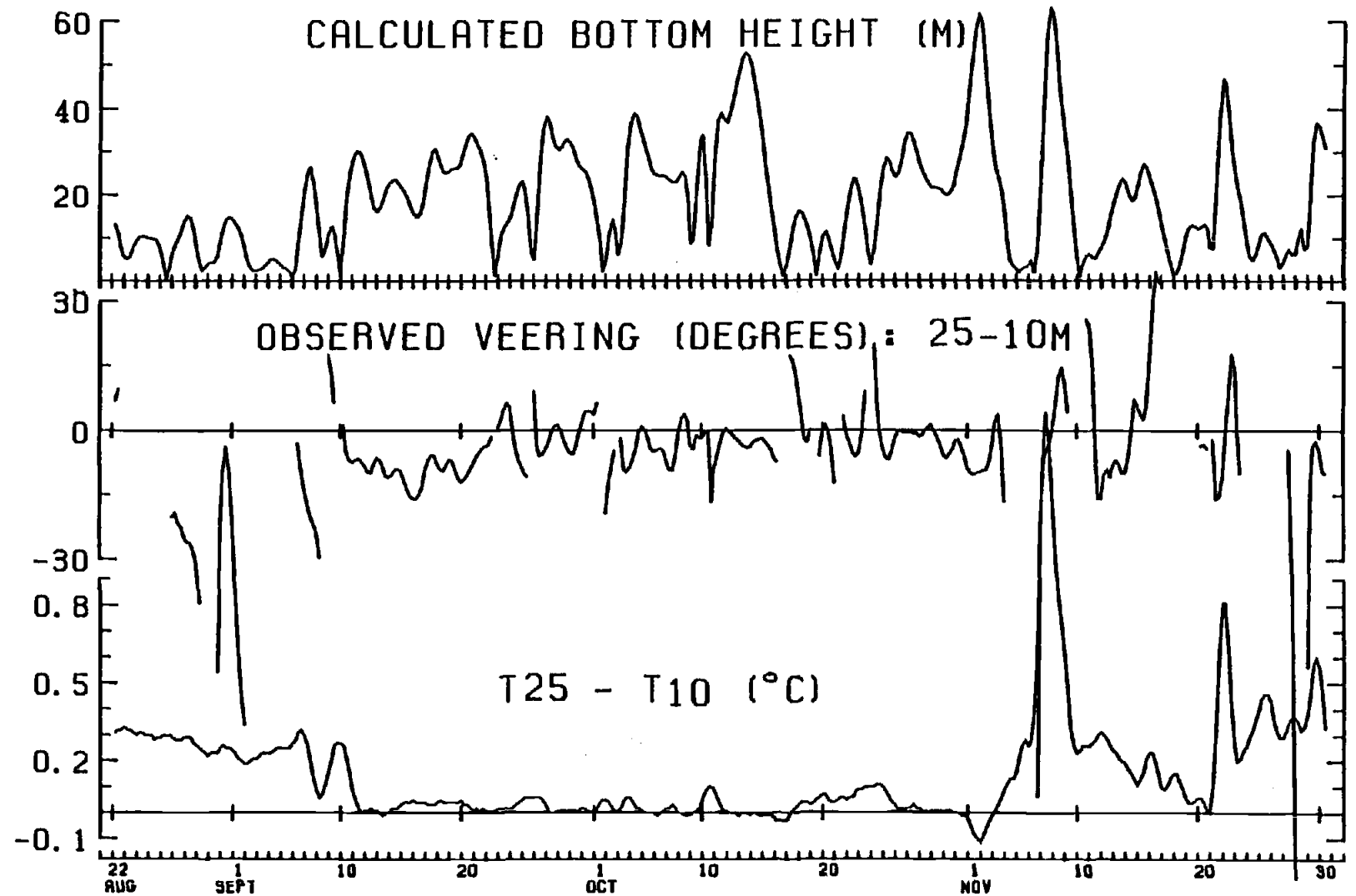

Figure 22. Calculated boundary layer height (meters); temperature difference (°C) and current vector veering (degrees) between 10 and 25 meters, not plotted if current velocities are <3 cm/s.

current meters was greater than 3 cm/s); and (3) the calculated height (σ_{BL}) of the BBL above the sea floor, generated from an equation (see page 67) which neglects the effects of stratification. The striking feature of the temperature difference time series is that ΔT was large during the "summer" (before 11 September) and the "winter" (from 7 November), but very small (<0.1° C) through the entire transition period from 11 September until the first week of November (Figure 22). During this period, the flow in the lower part of the water column was predominately poleward and strong (Figure 11). In theory, a stratified water column will develop a well-mixed, isothermal BBL with time (time scale $\leq 2\pi/f$) during steady current (Weatherly and Martin, 1978); thus, one would suspect the isothermal layer observed between 10 and 25 m during the transition period was a signature of a BBL associated with the strong poleward flow.

A test of the BBL hypothesis was made by calculating a time series of the angle (θ) of current veering between 25 and 10 m; a counterclockwise rotation with depth would be consistent with bottom Ekman-like veering. The time series of veering angle θ was obtained from

$$\theta = \tan^{-1} v_{10}/u_{10} - \tan^{-1} v_{25}/u_{25}$$

In this sense, a negative angle denotes counterclockwise veering with

depth, since eastward, northward, westward and southward flow is denoted by 0°, 90°, 180° and -90° respectively. To avoid meaningless noise, veering angles were displayed only when the speed at both instruments exceeded a threshold value, set at 3 cm/s in this case. Figure 22 shows that veering angle is highly variable in the "summer" and "winter" portions of the records, but relatively steady during the transitional period when most values were between 0° and -15°; the mean value for this period was -3.9°.

Although Kundu (1976; 1977) has shown from summer data that a consistent, small, negative angle between time series of bottom current vectors can be explained by the frictional boundary layer, it also seemed possible that the small difference in current veering between the two instruments might be the result of systematic measurement error. For this reason, we have examined the compass calibration data in detail (see Appendix). Of the four current meters, three exhibited very small differences (< 1.5°) between calibrations. However, at the deepest current meter, there was a systematic difference of ~5° between the calibrations before and immediately after the TURTLE deployment; the disagreement is in the sense that using the alternative calibration would increase the observed counterclockwise veering by ~5°.

The thickness of the BBL, σ_{BL}, was calculated from an equation which neglects the effects of stratification (Caldwell et al., 1976):

$$\sigma_{BL} \approx (0.4)u_*/f$$

where the friction velocity $u_* \approx (0.04)V_g$, f is the Coriolis parameter, and V_g is the magnitude of geostrophic velocity above the boundary layer, approximated in this case by the measured velocity at 25 m above the bottom. The composition of the sea floor near the mooring is very fine sand (Runge, 1966). Mean calculated BBL height (σ_{BL}) during the transitional period more than doubled the mean height during "summer" and was also larger than the height during "winter":

Season	Mean BBL Height
"summer"	8.9 m
"fall"	23.0 m
"winter"	18.3 m

On the event time scale, ~3-7 days, the BBL during "fall" was often above 30 m (Figure 22), which places it above the two near-bottom current meters at 10 and 25 m. A heightened BBL is caused in the calculation by large current velocities at 25 m, which in this case were northward.

Northward wind-forced currents were "boosted" at depth by the prevailing negative current shear, $-\partial v/\partial z$, yielding strong, deep, northward currents, often >20cm/s (Figure 11).

The BBL height was also determined from CTD casts closest to the mooring, where the height of the BBL was considered to extend upwards to the point where the temperature was within 0.05° of the temperature at the deepest part of the cast. Figures of the temperature casts are shown in Reid et al. (1985).

	21 Aug	22 Sept	29 Oct	18 Nov	2 Dec
CTD BBL (m)	11	31	25	10	11

CTD casts show that during the transitional period, the BBL height was two to three times larger than during the "summer" or "winter" period.

Evidence for the BBL Above 25 m

A visual inspection of Figure 22 shows large values of σ_{BL} were strongly associated with a small negative veering angle (θ) between 25 and 10 m, usually about 5°. It is also instructive to check for Ekman-like veering between 50 and 25 m (Figure 23). And indeed, small negative

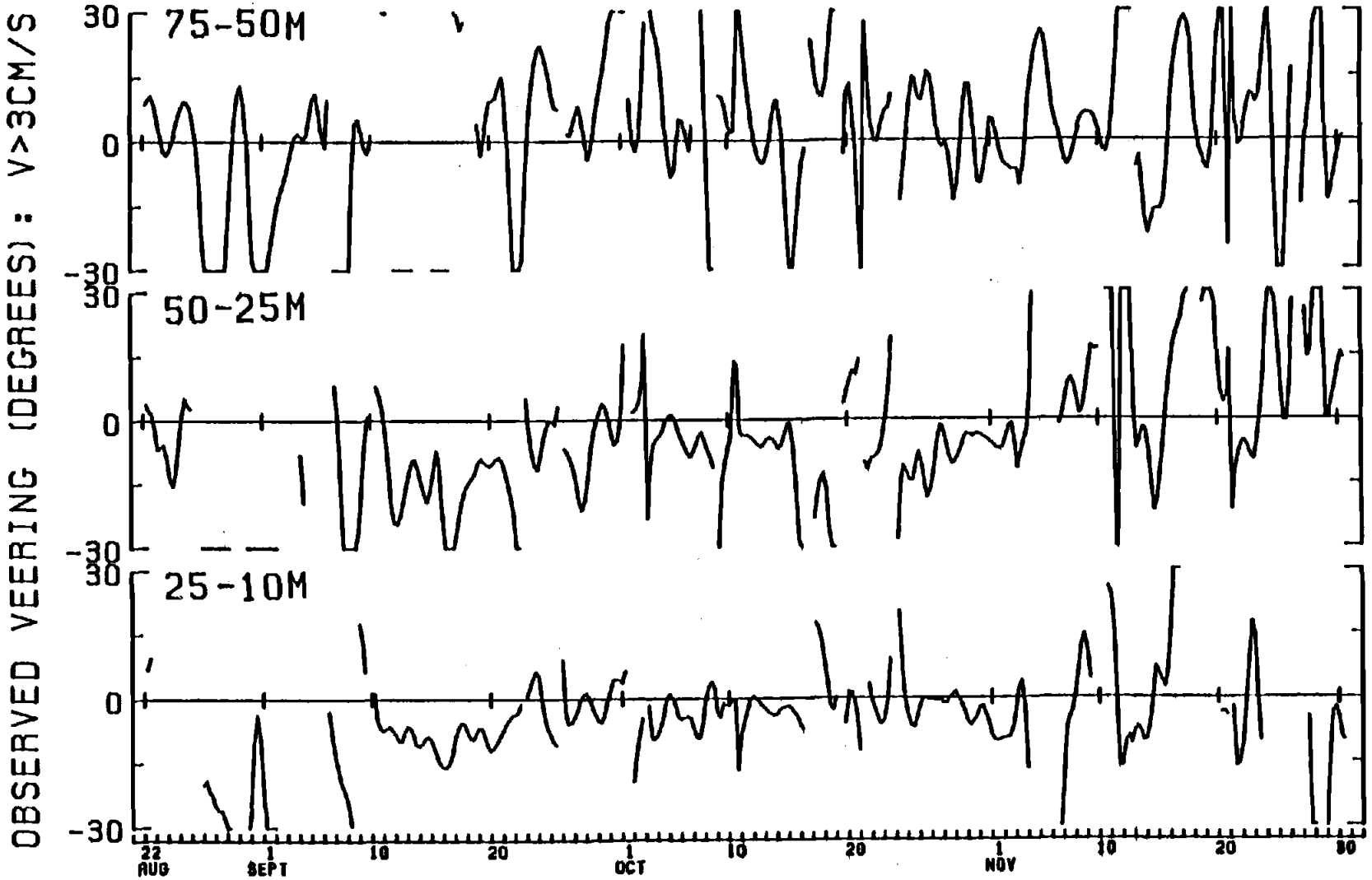

Figure 23. Time series of current vector veering between adjacent current meters. Not plotted for current velocities <3 cm/s; veering >30° plotted as 30°, veering <-30° plotted as -30°.

veering angles were apparent during "fall", especially during large bottom height events: e.g., on 11, 17-21, 26-28 September, 3-4, 11-14, 23-26 October and 31 October-2 November. This implies the top of the BBL extended between 25 and 50 m, and adds more evidence to the hypothesis that bottom boundary effects were important during the transition between summer and winter. Finally, a check was made for Ekman-like veering between 75 and 50 m (Figure 23). In general, extremely erratic veering was found at these heights. The BBL extending to these heights would be surprising because towards the surface the pycnocline would strongly resist the turbulence caused at the boundary. These results are consistent with the EOF analysis in Chapter 2 which showed that the first mode eigenvector resembles a surface Ekman layer top of a bottom Ekman layer.

Thermal Wind Effects and the BBL

It should be pointed out that in the presence of a "thermal wind" a counterclockwise rotation with depth could also occur. For instance, if there was a mean eastward current at all depths and a positive onshore density gradient, then deeper current vectors would be more northward and give a spurious impression of frictional veering. However, the mean alongshore current during "fall" (Table 4) was more northward at 25 m

than at 10 m, i.e., the shear between 25 and 10 m was opposed to the positive horizontal density gradients, therefore not consistent with thermal wind effects. A mean eastward current was apparent during "fall" at all four current meters, but was weak (0.2 cm/s) at the deepest current meter (Table 4).

The importance of current veering forced by horizontal density gradients was further checked by estimating $\partial\rho/\partial x$ from hydrographic data and the thermal wind relationship, $\partial v/\partial z=-(g/f\rho)(\partial\rho/\partial x)$, and comparing the calculations with $\partial v/\partial z$ observed at the current meter mooring. The calculations of $\partial v/\partial z$ at the current meter mooring used the shallowest and deepest current meters and were made at the time of the closest inshore and offshore CTD casts to the mooring: $\partial v/\partial z=(v_{31}-v_{96})/(z_{31}-z_{96})$. The calculations of $\partial\rho/\partial x$ were made from the closest CTD casts to either side of the mooring. Since the depth of the inshore cast was typically 70 m, isopycnals were extended at the same angle as the two CTD casts offshore of the mooring below 70 m. $\partial\rho/\partial x$ was subsequently converted to $\partial v/\partial z$ and vertically integrated between 31 and 96 m.

From Figure 5, during the 21 August section, i.e., before the fall

transition, the density gradient near the current meter, $\partial\rho/\partial x \approx 3.6\times10^{-10}$ gm cm^{-4}, giving a calculated current shear, $\partial v/\partial z \approx -3.3\times10^{-3}\ s^{-1}$, in excellent agreement with observed current shear at the current meter, $\partial v/\partial z \approx -3.3\times10^{-3}\ s^{-1}$. However, comparing hydrographic and measured shears from data during the transitional period show geostrophic effects during the 22 September section do not explain the observed shear: the estimated hydrographic density gradient, $\partial\rho/\partial x \approx 8.0\times10^{-11}$ gm cm^{-4}, giving a calculated current shear, $\partial v/\partial z \approx -7.5\times10^{-4}\ s^{-1}$, less than half the observed shear, $\partial v/\partial z \approx -1.6\times10^{-3}\ s^{-1}$. Likewise, during the 29 October section, $\partial\rho/\partial x \approx 1.7\times10^{-11}$ gm cm^{-4}, and $\partial v/\partial z \approx -1.6\times10^{-4}\ s^{-1}$, did not agree in sign with shear at the current meter, $\partial v/\partial z \approx 4.5\times10^{-4}\ s^{-1}$.

Complex Correlations

Kundu (1976) proposed a method for evaluating the phase angle of the complex correlation between two vector time series which weights the contributions of each vector and tends to average out the strong fluctuations during low current velocities. This method,

$\theta_{av}=\tan^{-1}(\langle u_1v_2-v_1u_2\rangle/\langle u_1u_2+v_1v_2\rangle)$, offers advantages over calculating mean instantaneous veering, $\theta_{av}=\langle\theta(t)\rangle=\langle(\tan^{-1}v_2/u_2)-(\tan^{-1}v_1/u_1)\rangle$; and over mean vector veering, $\theta_{av}=(\tan^{-1}(\langle v_2\rangle/\langle u_2\rangle)-\tan^{-1}(\langle v_1\rangle/\langle u_1\rangle))$, which may not be meaningful if mean currents are smaller than current fluctuations. The results of these three different calculations can be seen in Table 3a.

The calculations of phase angle support the picture of Ekman-like veering with a -4.7° angle between 25 and 10 m, as does the -3.6° angle between 50 and 25 m. The mean angle between 50 and 75 m was 1.7° clockwise with depth, or consistent with surface Ekman-like veering. The magnitude of the complex correlation increased with depth, signifying that phase differences between time series was more uniform at the deepest current meters. Table 3b shows the three different mean veerings for only the fall segment. In this table, the complex magnitudes increased between 10 and 25 m and between 25 and 50 m during "fall".

In Table 3, "v>", "n" and "mean" in the center of the table show the reasoning behind the "cut-off" criteria of not plotting currents less than 3 cm/s in Figure 22 and 23. There were 402 current meter observations at each current meter depth. We chose the cut-off value of 3 cm/s because it

Table 3a. Mean current vector veering: Complex correlation magnitude (CM) and phase angle (θ_{av}); veering of mean vector and mean instantaneous veering. The veering angle was calculated using different cutoff values for velocity ("v>") and is given in cm/s, the remaining number of observations was "n", and the mean of "n" observations was "mean"

Vectors	Complex Correlation		Instantaneous Mean Veering			Veering of MeanVector
	CM	θ_{av}	v>	n	mean	
25-10	0.94	-4.7°	0	402	-2.3°	-10.1°
			2	343	0.7°	
			3	301	-5.0°	
			4	266	-5.1°	
			5	245	-5.6°	
50-25	0.88	-3.6°	0	402	-7.4°	
			2	374	-4.5°	-7.4°
			3	349	-6.0°	
			4	319	-8.5°	
75-50	0.89	1.7°	0	402	-8.1°	-27.5°
			2	384	3.5°	
			3	370	-0.6°	
			4	352	-0.7°	

Table 3b. As above, but only calculated during the "fall segment".

Vectors	Complex Correlation		Instantaneous Mean Veering			Veering of MeanVector
	CM	θ_{av}	v>	n	mean	
25-10	0.98	-4.6°	0	402	0.7°	-6.0°
			2	215	0.1°	
			3	206	-3.9°	
			4	198	-3.8°	
			5	190	-4.2°	
50-25	0.95	-7.1°	0	402	-4.7°	-7.2°
			2	218	-6.5°	
			3	210	-7.6°	
			4	201	-8.8°	
75-50	0.87	3.7°	0	402	-9.5°	-1.3°
			2	215	6.4°	
			3	203	1.6°	
			4	190	1.6°	

mirrored the complex correlation values and left a reasonable number of observations.

In the last chapter it was stated that the poleward undercurrent rose in the water column with time. In connection with analysis done in this section one might also say that the BBL height rose in the water column to include the lower portion of the undercurrent, causing the poleward undercurrent's decrease near the bottom observed during the transition.

V. SEPARATION OF THE DATA ACCORDING TO REGIME

Statistics of the low-passed data have been subdivided into three segments (Table 4): "summer" which lasted through 10 September; "fall" began on 11 September and lasted through 6 November; and "winter" starting on 7 November and continuing until the end of the mooring data on 30 November.

Regime	Date
Summer	22 August - 10 September 1980
Fall Transition	11 September - 6 November 1980
Winter	7 November - 30 November 1980

The justification for the dates of these subdivisions are discussed in the two previous chapters. Figures 24 through 28 are taken from the statistics in Table 4. Table 5 shows the correlation coefficients for only the fall period; these correlations are very similar to Table 2 and are shown here as a counterpoint to the correlations of summer and winter regime data in Huyer et al. (1978)

Table 4. Statistics of the low-passed data of the three regimes.

			Summer	Fall	Winter
$\bar{v}$	31 m	(cm/s)	-16.4	4.6	9.4
	56 m	(cm/s)	-7.8	9.3	8.3
	81 m	(cm/s)	1.3	11.0	3.3
	96 m	(cm/s)	3.1	8.8	1.1
	Wind	(m/s)	-1.2	0.8	1.7
	$\bar{\tau}_y$	(dyne/cm^2)	-0.05	0.09	0.28
v_{SD}	31 m	(cm/s)	5.6	13.7	23.2
	56 m	(cm/s)	6.3	12.3	21.1
	81 m	(cm/s)	6.4	12.4	14.1
	96 m	(cm/s)	5.8	10.8	5.9
	Wind	(m/s)	2.4	3.0	3.3
	$\tau_{y_{SD}}$	(dyne/cm^2)	0.12	0.30	0.65
$\bar{u}$	31 m	(cm/s)	-0.9	1.3	1.3
	56 m	(cm/s)	0.3	2.4	1.8
	81 m	(cm/s)	1.2	1.4	1.1
	96 m	(cm/s)	-0.3	0.2	-0.1
	Wind	(m/s)	0.3	-0.1	0.2
	$\bar{\tau}_x$	(dyne/cm^2)	0.01	0.01	0.18
u_{SD}	31 m	(cm/s)	1.9	4.0	9.1
	56 m	(cm/s)	2.5	3.5	4.6
	81 m	(cm/s)	1.9	2.2	3.3
	96 m	(cm/s)	0.9	1.7	1.8
	Wind	(m/s)	0.6	1.6	3.5
	$\tau_{x_{SD}}$	(dyne/cm^2)	0.02	0.14	0.57
$\bar{T}$	31 m	(°C)	8.26	9.41	12.53
	56 m	(°C)	7.98	8.37	10.94
	81 m	(°C)	7.72	8.03	9.08
	96 m	(°C)	7.47	7.99	8.74
T_{SD}	31 m	(°C)	0.05	1.24	0.48
	56 m	(°C)	0.08	0.62	0.92
	81 m	(°C)	0.14	0.34	0.56
	96 m	(°C)	0.18	0.30	0.30
Principal Axis	31 m	(°T)	5.3	6.6	-7.0
	56 m	(°T)	15.9	12.8	6.6
	81 m	(°T)	10.6	3.2	8.8
	96 m	(°T)	1.5	3.2	4.3
	Wind	(°T)	5.4	12.7	42.0
Adjusted sea level	$\bar{\eta}$	(cm)	285.5	291.1	298.9
	η_{SD}	(cm)	2.3	5.5	6.8

Table 5. Correlation coefficients between linearly detrended time series for the "fall" period from 11 September to 6 November (229 six-hourly observations). "CC_m" and "CC_0" are the maximum and zero lag correlation coefficient, respectively. "Lag" is the time in hours of the maximum correlation; positive values of "lag" indicate that the column header leads. "ν" is the degrees of freedom. Correlations are flagged that are below the 95% (•) and 99% (*) significance levels.

	Alongshore Wind				Adjusted Sea Level				Onshore Wind			
	CC_m	CC_0	Lag(hr)	ν	CC_m	CC_0	Lag(hr)	ν	CC_m	CC_0	Lag(hr)	ν
V Current												
31m	0.73	0.57	+(12,18)	18	0.83		0	23	0.57		0	33
56m	0.67	0.51*	+(12,18)	21	0.83		0	25	0.57		0	33
81m	0.70	0.50*	+(18)	23	0.82		0	21	0.49		0	38
96m	0.67	0.48*	+(18)	21	0.79		0	23	0.48		0	38
Sea level	0.75	0.64	+(12)	29					0.65		0	38
V_{31}-V_{96}	0.38*	0.36•	+(6)	29	0.35•		0	29	0.40		0	46
U Current												
31m	0.42	0.00•	+(42)	38	0.36*	0.22•	+(18,24)	33	0.20•	0.20•	−(0,6)	46
56m	0.54	0.20•	+(24,30)	29	0.67	0.63	+(6,12)	23	0.39*	0.39*	−(0,6)	33
81m	0.59	0.06•	+(30)	23	0.71	0.55*	+(18)	19	0.48	0.38*	+(12,18)	29
96m	0.48*	−0.36•	+(42)	23	0.46	0.08•	+(24)	33	0.34*	0.03•	+(24)	46
Temperature												
31m	0.31•	0.28•	+(18,24)	29	0.28•		0	18	0.15•		0	29
56m	0.32•		0	19	0.28•		0	11	0.30•		0	21
81m	0.29•		0	23	0.26•		0	14	0.19•		0	25
96m	0.41*	0.24•	+(30,36,42)	33	0.49*	0.42•	+(18)	19	0.29•	0.28•	+(6,12)	38

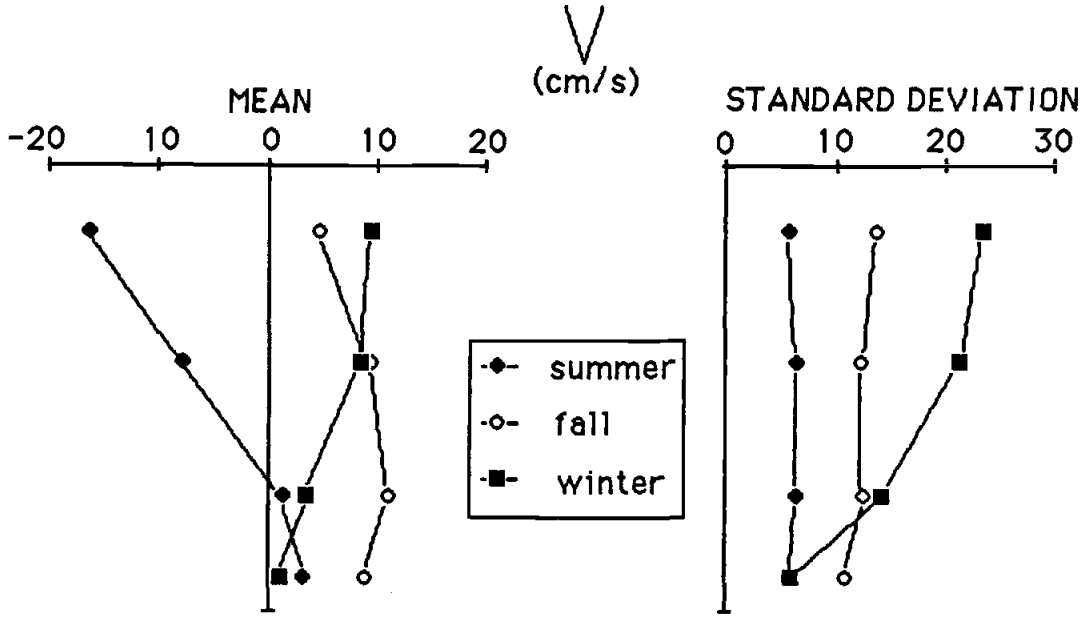

Figure 24. Seasonal variation of alongshore means and standard deviations with depth at 31, 56, 81 and 96 m.

Mean alongshore currents (Figure 24) during summer were poleward with depth and there was a zero crossing between 56 and 81 m. Currents were southward at 31 and 56 m and northward at 81 and 96 m. Standard deviations during summer were almost constant with depth, varying by only 0.6 cm/s. In winter, currents were equatorward with depth, with no zero crossing; standard deviations decreased with depth. Fall means were northward and increased with depth between 31 and 81 m; standard deviations were constant with depth, like summer, but the magnitude of the standard deviations were twice as strong as summer.

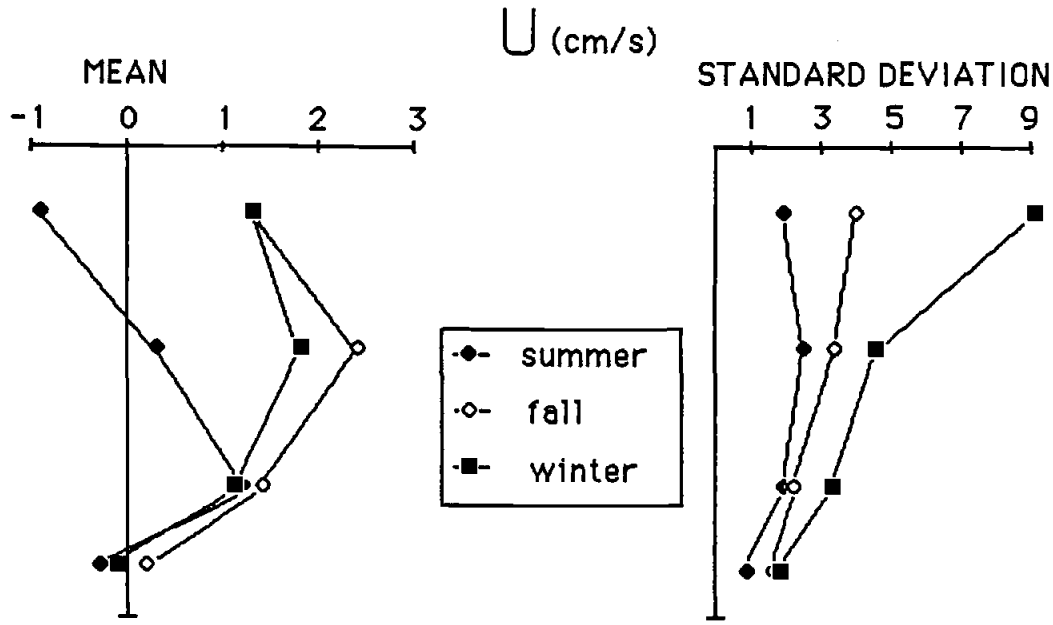

Figure 25. Seasonal variation of onshore-offshore mean currents and standard deviations with depth at 31, 56, 81 and 96 m.

Onshore-offshore mean currents (Figure 25) during summer were offshore at 31 and 96 m and onshore at the intermediate depths of 56 and 81 m, suggesting that the onshore currents at 56 and 81 m were part of the "geostrophic interior", found between the surface and bottom Ekman offshore flow layers (Kundu, 1977; Huyer, 1983). During winter, means were onshore at the three shallowest current m and weakly offshore at 96 m; standard deviations decreased with depth. During fall, means were onshore at all depths; standard deviations decreased with depth.

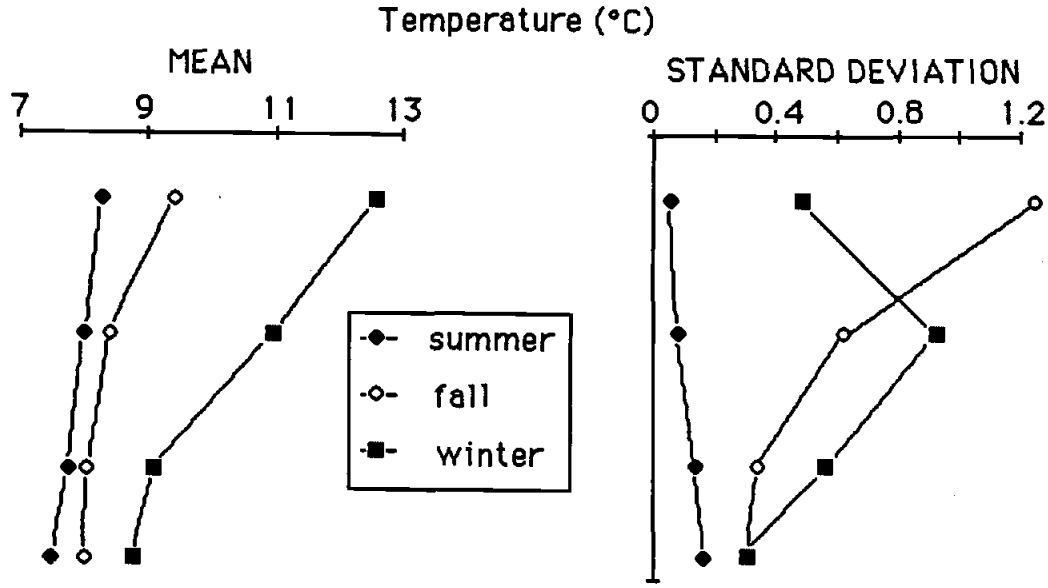

Figure 26. Seasonal variation of temperature means and standard deviations with depth at 31, 56, 81 and 96 m.

Temperature means (Figure 26) decreased with depth during all seasons. Temperatures means increased from summer through winter at all depths. Temperature standard deviations increased slightly with depth during summer and decreased strongly with depth during fall. Fall and winter's standard deviations were much stronger than during summer. The strongest standard deviation was at 96 m during summer, at 31 m during fall and at 56 m during winter.

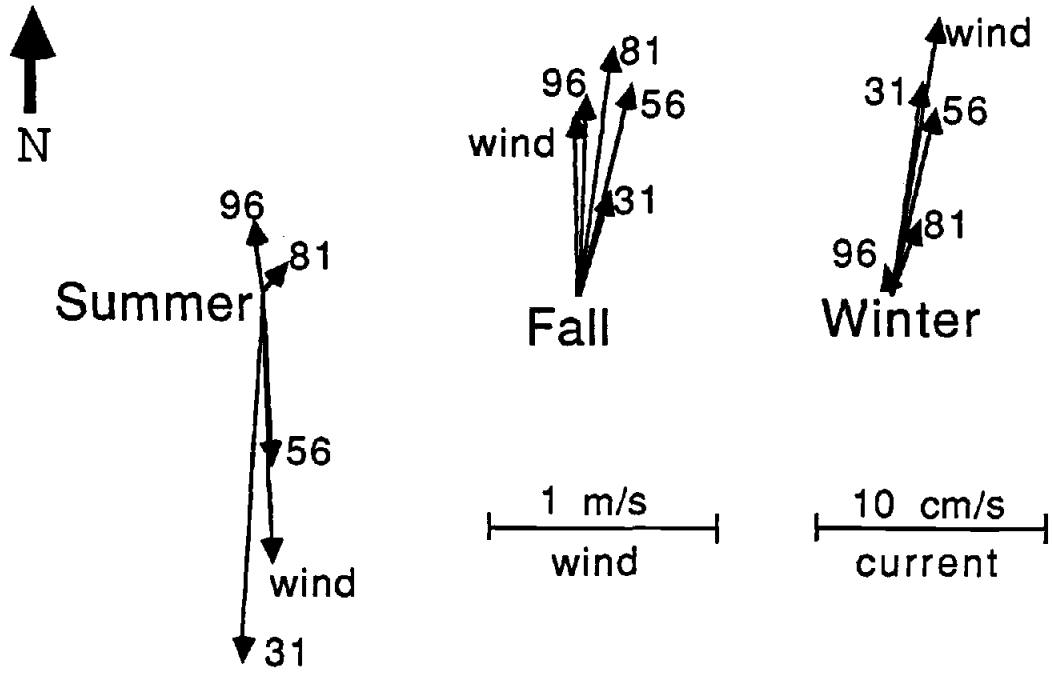

Figure 27. Seasonal vector means of currents and Newport wind.

During summer, mean current vectors (Figure 27) spiraled 180° counterclockwise with depth; near-surface current was southward and near-bottom current was northward. During fall, current vectors also rotated counterclockwise with depth, but the angle of rotation was small (14.5°). The poleward undercurrent during summer was apparent at 81 and 96 m; during fall the undercurrent rose to include the current meter at 56 m. During winter, current vector magnitudes at 31 and 56 m were twice as large as at 81 m and five times as large as at 96 m. During summer and winter, the strongest mean current vectors were at the surface; during fall, the strongest means were towards the bottom.

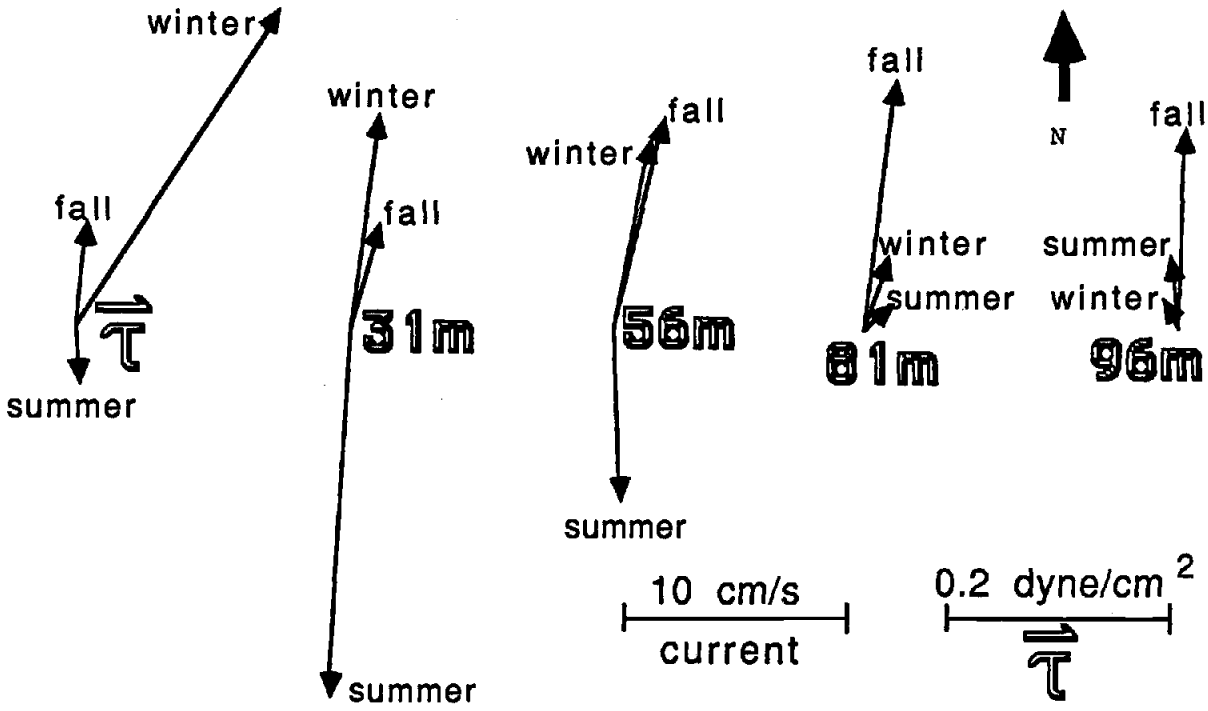

Figure 28. Vector means of wind stress (τ) and currents at TURTLE.

The largest rotations of mean current vectors at 31 and 56 m and with wind stress (τ) occurred between summer and fall (Figure 28), as mean vectors rotated from southwards to northwards. From fall to winter, mean vectors of wind stress and 31 m current increased in magnitude. Currents at 56 m had very similar mean vectors during winter and fall. At the two deepest current meters, mean currents were weak (and generally northward) during summer and winter. During fall, currents at the two deepest current meters were strongly northward and much stronger than during either summer or winter.

VI. SUMMARY AND CONCLUSIONS

Several hypotheses about the fall transition were mentioned in the INTRODUCTION and discussed in the following chapters. The questions will be explicitly answered here.

Did the southward surface current decay suddenly, as a result of a single strong northward wind event? Near-surface currents at the mooring did not decay as a result of single strong wind stress wind event; rather, a series of modest wind events of comparable magnitude and duration in late summer were implicated with the decay of southward current. The northward wind event associated with the initial appearance of northward near-surface current lasted only one day and had a peak velocity less than 4 m/s.

Would southward surface currents disappear even if there were no northward wind events in late summer and fall? This hypothesis was not tested in this thesis and an answer was not attempted. The implication of the question is whether the transition was forced by local wind events or by continental shelf waves that propagated from other locations. The spring transition is typically a quick and dramatic event; Huyer et al. (1979) have shown that the spring transition can be explained by local effects. In

contrast, the transition of oceanic parameters during fall (e.g. alongshore current shear, the hydrographic regime, sea level and currents) was achieved gradually over a longer time scale. If one assumes that the fall transition was similar elsewhere along the west coast of North America then one can speculate that shelf waves were not likely to be generated from such gradual effects and were therefore not responsible for the transition.

Did the southward surface current decay very gradually by dissipation? Was the southward surface current replaced by northward surface flow in incremental steps through a series of northward wind events which are common in fall? We have no evidence that internal frictional dissipation played a role in the decay of the southward surface current. Instead, it seemed to decay as a result of variations in the wind. The first month of observations show that surface current gradually weakened through a series of northward events that were more poleward than the last. The decay was achieved in three ways: first, in a reversal of a phenomenon observed during summer, the effects of northward winds were stronger than the effects of southward winds on near-surface current; second, northward wind events of early fall, even though comparable in magnitude and duration, were forcing progressively stronger current

fluctuations; and third, later northward wind events of fall were stronger than the earlier wind events and forced the continuing trend of increasing poleward near-surface current.

Regression analysis of sea level and near-surface alongshore current show the two parameters strongly tied. Northward near-surface flow was associated with sea level above its historical long-time mean, and southward near-surface flow was associated with sea level below its long-time mean. In addition, sea level was implicated in the transition of southward near-surface flow to northward flow beginning on 11 September; previous to 11 September it is believed that northward near-surface flow did not develop during northward wind stress events because coastal sea level was too low, i.e., $\partial\eta/\partial x < 0$.

Did the winter northward flow regime result from the surfacing of the undercurrent? The surfacing of the undercurrent was quite gradual. Time series of current shear between adjacent current meters show that the undercurrent moved above the deepest current meter during the middle of September; and not above the current at 56 m until 10 October. The transition of near-surface currents at 31 m seemed a separate process that started a month before the poleward undercurrent had risen to 56 m.

Was the fall transition achieved primarily by means of a change in

the offshore density gradients, as appears to be the case during the spring transition? Clearly, the beginning of the winter regime (and the end of the fall transition) was achieved with the leveling of the frontal layer in early November. During this event, northward wind stress caused dramatic changes in alongshore shear, sea level, onshore and offshore currents as well as the density field. The transitional period was marked by gradual trends of sea level, alongshore current shear, alongshore surface current and the rising of the poleward undercurrent. The changes of these parameters during the fall probably *are* tied to gradual changes in offshore density structure (e.g. alongshore current shear, which is certainly related to density effects through the thermal wind relationship), but the linkage of the dynamics is not clear. Moreover, the appearance of a heightened bottom boundary layer during fall was definitely not tied to density effects.

Were the current fluctuations associated with the transition primarily barotropic or baroclinic in nature? Standard deviations of alongshore currents during fall were twice as large as standard deviations during summer. They were, like summer, very depth-independent, i.e., barotropic. The mean flow during the first month of the transition showed decreasing baroclinic effects, with a gradual trend towards decreasing current shear. The mean flow during the second month of the transition

was barotropic, with currents at all depths flowing in unison. Mean northward and onshore currents during fall were similar to the winter regime.

The end of the fall transition on 6 November occurred in response to a long period of northward wind stress punctuated by two large wind events. The ocean reacted to the wind events with high onshore current flow which leveled and lowered the frontal layer over the shelf. The winter regime's signature appeared in the large rise of current temperature at the mooring, in high sea level at the coast and in baroclinic alongshore current fluctuations.

The end of the fall transition contained a strong signal, with dramatic changes of the above mentioned oceanic variables. The time of the beginning of the transition was more uncertain, because of the gradual changes occurring in late summer and early fall. It may be that the concatenation of events at the end of the summer regime was fortuitous; whether the series of events on 11 September were truly linked and not nuances of this data set, is hard to answer. Nevertheless, the simultaneous events on 11 September are listed here:

(1) a northward wind event forced northward near-surface flow; before 11 September, no northward wind events were associated with northward current flow; after 11 September, **all** northward wind events were associated with northward surface currents,

(2) coastal sea level rose to its historical long-time mean; before 11 September, sea level was always below its historical mean, afterwards sea level fluctuated above and below it,

(3) the poleward undercurrent rose off the bottom and became strongest at 81 m at the mooring,

(4) the appearance of a large bottom boundary layer at the mooring that persisted during the entire transitional period.

The transitional leveling of the density field was gradual. Each successive hydrographic section, taken approximately monthly, shows isopycnals less inclined. Time series of alongshore current shear, a good measure of the local isopycnal inclination, supports the notion of a gradually lessening frontal layer.

The appearance of a large bottom boundary layer persisted during the entire transitional period. Forcing of the heightened bottom boundary layer was through the combined effects of negative current shear and the strong northward wind events during fall. The results were strong deep northward current velocities. The signature of the bottom boundary layer

was apparent in these relationships:

(1) an isothermal layer between the two deepest current meters,

(2) a persistent, small, counterclockwise with depth veering angle of current vectors between 81 and 96 m, and between 56 and 81 m, seen in both the time series of veering angle and in the complex correlations,

(3) a calculated mean BBL height approximately 23 m

(4) and profiles of temperature from CTD casts near the mooring indicate a BBL two to three times larger during the transition than during the "summer" or "winter".

Hydrographic estimates of current shear indicate the veering was not explained geostrophically, suggesting its source was frictional bottom dynamics.

The very large bottom boundary layer and the slow rise of the poleward undercurrent through the water column are unique features of the transition period that have not been observed during other seasons; these two phenomena may be linked.

BIBLIOGRAPHY

Allen, J.S. and P.K. Kundu. 1978. On the momentum, vorticity, and mass balance on the Oregon Shelf. J. Phys. Oceanogr., Vol. 8(1):13-2.

Anderson, I., A. Huyer and R.L. Smith. 1983. Near-inertial motions off the Oregon Coast. J. of Geophys. Res. Vol. 88, No. C10: 5960-5972.

Bakun, A. 1972. The Peg upwelling index off Oregon during 1972, CUE *Notes*, no. 10, pp. 8-12l, Oregon State Univ., School of Oceanography.

Bendat, J.S. and A.G. Piersol. 1971. Random Data: Analysis and Measurement Procedures, 407 pp., John Wiley, New York.

Bourke, R.H. 1972. Ph.D thesis. A study of the seasonal variation in temperature and salinity along the Oregon-Northern California Coast. Dept. of Oceanography, Oregon State University.

Brink, K.H., D.W. Stewart, and J.C. Van Leer. 1984. Observations of the coastal upwelling region near 34°30'N off California; Spring 1981. J. Phys. Oceanogr., Vol. 14, 378-391.

Brunson, B.A. 1973. M.S. thesis. Steric contributions to the seasonal oscillation in sea level off Oregon. Dept. of Oceanography, Oregon State Univ.

Burt, W.V. and B. Wyatt. 1965. Drift bottle observations of the Davidson Current off Oregon. Studies on Oceanography. Kozo Yoshida, editor. University of Washington Press.

Caldwell, D.R., C.W. Van Atta and K.N. Helland. (1972). A laboratory study of the turbulent Ekman layer. Geophysical Fluid Dynamics, 3, 125-160.

Collins, C.A. 1964. M.S. thesis. Structure and kinematics of the permanent oceanic front off the Oregon coast. Dept. of Oceanography, Oregon State Univ.

Collins, C.A. 1967. Ph.D thesis. Description of measurements of current velocity and temperature over the Oregon continental shelf, July 1965-February 1966. Dept. of Oceanography, Oregon State Univ.

Davis, R.E. 1976. Predictability of sea surface temperatures and sea level pressure anomalies over the North Pacific Ocean. J. Phys. Oceanogr., Vol. 6, 249-266.

Denbo, D.W., K. Polzin, J.S. Allen, A. Huyer and R.L. Smith. 1984. Current meter observations over the continental shelf off Oregon and California, February 1981 - January 1984. College of Oceanography, Oregon State Univ., Data Report 112, Ref. 84-12.

Dodimead, A.H., F. Favorite, and T. Hirano. 1963. Review of oceanography of the Eastern Subarctic Pacific. J. Fish. Res. Bd. Can. 24(11):2207-2227.

Fofonoff, N.P. 1969. Spectral characteristics of internal waves in the ocean. Deep-Sea Research, Supplement to Volume 16: 58-71.

Garratt, J.R. 1977. Computation of surface fluxes from climatological and synoptic data. Monthly Weather Review, V. 105, January: 915-929.

Halpern, D. 1976. Structure of a coastal upwelling event observed off Oregon during July 1973. Deep-Sea Res., 23:495-508.

Halpern, D., R.L. Smith and R.K. Reed. 1978. On the California Undercurrent over the continental slope off Oregon. J. of Geophys. Res. Vol. 83, no. C3: 1366-1372.

Huyer, A. 1977. Seasonal variation in temperature, salinity and density over the continental shelf off Oregon. Limnology and Oceanography, 22:442-453.

Huyer, A. 1983. Coastal Upwelling in the California Current System. Prog. Oceanog., Vol. 12. pp. 259-284.

Huyer, A., R.D. Pillsbury and R.L. Smith. 1975. Seasonal variation of the alongshore velocity field over the continental shelf off Oregon. Limnology and Oceanography, 20:90-95.

Huyer, A., R.L. Smith and E.J.C. Sobey. 1978. Seasonal differences in low-frequency current fluctuations over the Oregon Continental Shelf. J. of Geophysical Research, 83(C10):5077-5089.

Huyer, A., E.J.C. Sobey and R.L. Smith. 1979. The Spring transition in currents over the Oregon continental shelf. J. of Geophysical Research, 84(C11):6995-7011.

Kundu, P.K. 1976. Ekman veering observed near the ocean bottom, J. Phys. Oceanogr., Vol. 6, 238-242.

Kundu, P.K. 1977. On the importance of friction in two typical continental waters: off Oregon and Spanish Sahara. In: Bottom turbulence, J.C.J. Nihoul, editor, 8th Liége Colloquium on Ocean Hydrodynamics (1976). Elsevier Scientific Publishing Company. 309 pp.

Kundu, P.K., J.S. Allen and R.L. Smith. 1975. Modal decompostion of the velocity field near the Oregon Coast. J. Phys. Oceanogr., Vol. 5: 683-704.

Kundu, P.K. and J.S. Allen. 1976. Some three-dimensional characteristics of low-frequency fluctuations near the Oregon Coast. J. Phys. Oceanogr., Vol. 6:181-199.

Marthaler, J.G. 1977. M.S. Thesis. Comparison of sea level and currents off the Oregon coast using mean monthly data. School of Oceanography, Oregon State Univ.

Mooers, C.N.K., C.A. Collins and R.L. Smith. 1976. The dynamic structure of the frontal zone in the coastal upwelling region off Oregon. J. Phys. Oceanogr., Vol. 6(1):3-21.

Pillsbury, R.D., J.S. Bottero, R.E. Still and W.E. Gilbert. 1974. A compilation of observations from moored current meters. Volume VII. Oregon Continental Shelf, July-August 1973. School of Oceanography, Oregon State Univ., Data Report 58, Ref 74-9.

Pittock, H.L., W.E. Gilbert, A. Huyer and R.L. Smith. 1982. Observations of sea level, wind and atmospheric pressure at Newport, Oregon, 1967-1980. School of Oceanography, Oregon State Univ., Data Report 98, Ref. 82-12.

Reid, B., R.E. Schramm, A. Huyer and R.L. Smith. 1985. Current and CTD observations off Oregon: August to December 1980. College of Oceanography, Oregon State Univ., Data Report 116, Ref. 85-7.

Reid, J.L. and A.W. Mantyla. 1976. The effect of geostrophic flow upon coastal sea elevations in the northern North Pacific Ocean. J. Geophys. Res. 81(18):3100-3110.

Runge, E.J., Jr. 1966. M.S. thesis. Continental shelf sediments, Columbia River to Cape Blanco, Oregon. School of Oceanography, Oregon State Univ.

Sakou, T. and S. Neshyba. 1972. The temporal structure of oceanic motion off the Oregon coast, Northeastern Pacific, 1969. J. of Marine Res. Vol 30, no. 1: 1-14.

Smith, R.L. 1974. A description of current, wind and sea level variations during coastal upwelling off the Oregon Coast, July - August 1972. J. Geophys. Res., 79:435-443.

Sobey, E.J.C. 1977. Ph.D thesis. The response of Oregon shelf waters to wind fluctuations: Differences and transition between winter and summer. School of Oceanography, Oregon State Univ.

Strub, P.T., J.S. Allen, A. Huyer and R.L. Smith. 1987. Large-scale structure of the Spring Transition. J. Geophys. Res. In press.

Sverdurp, H.U., M.W. Johnson, and R.H. Fleming. 1942. The oceans: their physics, chemistry, and general biology. Englewood Cliffs, New Jersey, Prentice-Hall. 1087 p.

Tully, J.P. 1964. Oceanographic regions and processes in the seasonal zone of the North Pacific Ocean. Studies on Oceanography, pp 68 to 84. Kozo Yoshida, editor. University of Washington Press.

Weatherly, G.L. 1972. A study of the bottom boundary layer of the Florida Current. J. Phys. Oceanogr., Vol. 2: 54-72.

Weatherly, G.L. 1975. A numerical study of time-dependent turbulent Ekman layers over horizontal and sloping bottoms. J. Phys. Oceanogr., Vol. 5: 288-299.

Weatherly, G.L. and P.J. Martin. 1978. On the structure and dynamics of the oceanic bottom boundary layer. J. Phys. Oceanogr., Vol. 8: 557-570.

Wyatt, B., W.V. Burt and J.G. Pattullo. 1972. Surface currents off Oregon as determined from drift bottle returns. J. Phys. Oceanogr. Vol. 2(3): 286-293

APPENDIX

APPENDIX

Current Meter Compass Calibration

Calibration of the Aanderaa RCM4 magnetic compass consists of rotating the compass's vane through 360° and measuring the corresponding analog direction value (Pillsbury et al., 1974). Assuming there is no "dead zone" the 360° is divided evenly into 1024 units, so that one unit δ =

$$360°/1024 = 0.3516°$$

If δ is the analog direction (bit) value the instrument vane points $(0.3516\ \delta)°$ clockwise from magnetic north. The direction (θ) toward which the current is flowing relative to true north (Figure 29) is

$$\theta = (0.3516\ \delta)° + \text{local magnetic variation}$$

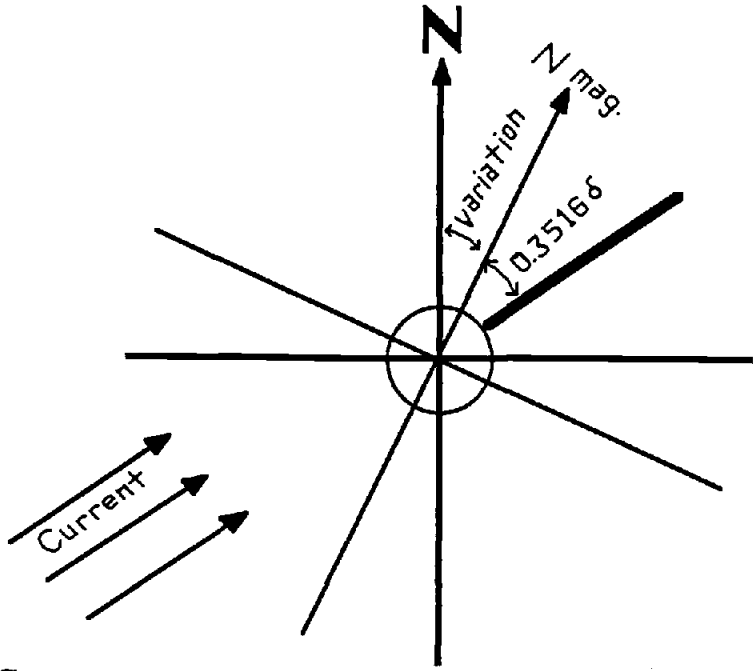

Figure 29. Current direction's relation to analog direction value, δ.

The potentiometer has a dead angle zone of about 3°. In this zone, there will be no contact, the reading is uncertain and the current meter automatically reads $\delta = 1023$.

A look-up table of raw bit number versus direction is prepared, taking into account the magnetic variations (declination) at the calibration site and at the installation site. Data is processed by linear interpolation between look-up table values.

Look-up tables of bit value versus direction for current meters used during the "Fall Transition Experiment" are shown in Tables 5, 6, 7 and 8 for current meters at depths of 96, 81, 56 and 31 m, respectively.

The 12/17/80 calibration (which was used to calibrate the data for this experiment) at 96 m differed from the previous calibration on 4/17/80 by a mean of 14 bits, which corresponds to ~5° (Table 6, column 4, bottom row). The difference is important because the observed angle of veering between 81 and 96 m was consistently a small, counterclockwise with depth veering angle, also ~5°.

Cardinal points of the compass from Table 6 corresponding to the 4/17/80 and 12/17/80 calibrations are shown in Figure 30. Imagine that the true current was due north and the true analog bit value for northward current was 472. From Figure 30, using the 12/17/80 calibration, a bit

current was 472. From Figure 30, using the 12/17/80 calibration, a bit number of 472 would also indicate due north. However, the 4/17/80 calibration would indicate current direction about 5° counterclockwise of north. In general, current data processed with the 4/17/80 calibration would result in current direction rotated about 5° counterclockwise of the 12/17/80 calibration. Therefore, using the 12/17/80 calibration (perhaps) systematically underestimates the veering angle between 81 and 96 m (if the 4/17/80 calibration was a more accurate measure of true current direction, which is impossible to ascertain). But more importantly, either calibration does not qualitatively negate the direction of veering: counterclockwise with depth.

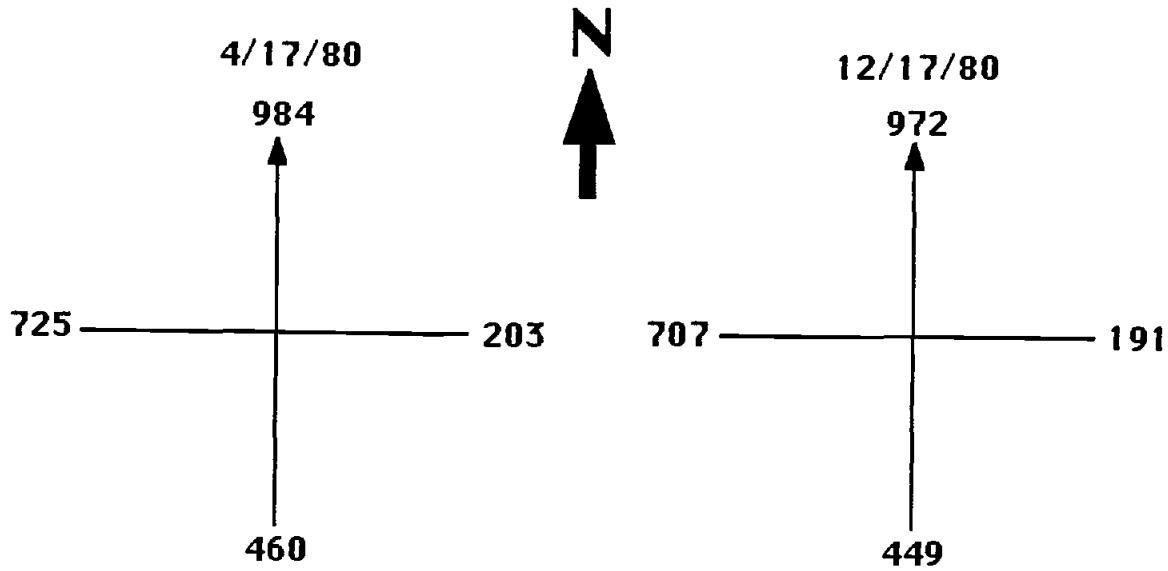

Figure 30. Cardinal compass points for the 4/17/80 and 12/17/80 calibration. The 12/17/80 calibration was used for this experiment.

Calibrations of the other current meter's compasses (81, 56 and 31 m, see Tables 7, 8 and 9) did not have large mean bit differences between calibrations; the largest difference was at 31 m between the 9/26/78 and 3/25/80 calibration with a mean difference of 4 bits (1.4°) which is an acceptable error. Since calibration differences were otherwise small, the accuracy of the compasses at 81, 56 and 31 m were not questioned.

Table 6. Calibration of bit value versus direction for current meter compass at 96 m. The first column (°T) shows degrees true (0°,90°,180° and 270° denoting north, east, south and west), the next two columns give the bit calibrations at 10° increments on the date shown above the column. The last column gives the differences between the bit calibrations between the second and the third column (C2-C3).The date of the calibration is starred if it was used to process the data of this experiment.

°T	4/17/80	12/17/80*	C2-C3
0	984	972	12
10	1014	1001	13
20	4	1023	5
30	32	20	12
40	61	50	11
50	90	78	12
60	118	107	11
70	147	135	12
80	174	163	11
90	203	192	12
100	231	191	12
110	260	249	11
120	289	278	11
130	317	306	11
140	346	335	11
150	375	363	12
160	403	391	12
170	433	420	13
180	462	449	13
190	491	478	13
200	521	506	15
210	550	535	15
220	579	564	15
230	609	593	16
240	638	622	16
250	667	649	18
260	695	677	18
270	725	707	18
280	755	736	19
290	784	766	18
300	814	795	19
310	844	826	18
320	871	854	17
330	899	883	16
340	927	912	15
350	956	940	14
Mean	536	522	14
Tape#	4044/1	4044/6	4044/15

Table 7. Calibration of bit value versus direction for current meter compass at 81 m. The first column (°T) shows degrees true (0°,90°,180° and 270° denoting north, east, south and west), the next three columns give the bit calibrations at 10° increments on the date shown above the column. The last three columns give the differences between bit calibrations of the columns. The date of the calibration is starred if it was used to process the data for this experiment.

°T	5/7/80	12/17/80*	7/9/81	C2-C3	C4-C3	C2-C4
180	450	453	448	-3	-5	2
190	480	484	478	-4	-6	2
200	510	514	508	-4	-6	2
210	538	543	537	-5	-6	1
220	568	572	567	-4	-5	1
230	598	602	596	-4	-6	2
240	628	631	626	-3	-5	2
250	656	661	656	-5	-5	0
260	685	688	684	-3	-4	1
270	713	718	714	-5	-4	-1
280	743	749	743	-4	-4	0
290	773	778	774	-5	-6	-1
300	801	806	802	-5	-4	-1
310	828	833	829	-5	-4	-1
320	857	863	857	-6	-6	0
330	885	885	888	0	3	0
340	915	914	917	1	3	-2
350	944	943	947	1	4	-3
0	973	972	976	1	4	-3
10	1001	1001	1005	0	4	-4
20	1023	1023	1023	0	0	0
30	15	17	17	-2	0	-2
40	43	45	47	-2	2	-4
50	73	75	76	-2	1	-1
60	102	105	106	-3	1	-4
70	131	133	134	-2	1	-3
80	160	162	162	-2	0	-2
90	190	196	190	-6	-6	0
100	219	225	220	-6	-5	-1
110	249	253	248	-4	-5	1
120	279	283	278	-4	-5	1
130	307	312	307	-5	-5	0
140	335	339	335	-4	-4	0
150	364	368	363	-4	-5	1
160	393	397	392	-4	-5	1
170	420	424	420	-4	-4	0
Mean	522	525	522	-3	-3	0
Tape#	4045/4	4045/9	4045/13			

Table 8. Calibration of bit value versus direction for current meter compass at 56 m. The first column (°T) shows degrees true (0°,90°,180° and 270° denoting north, east, south and west), the next two columns give the bit calibrations at 10° increments on the date shown above the column. The last column gives the differences between the bit calibrations between the second and the third column (C2-C3).The date of the calibration is starred if it was used to process the data of this experiment.

°T	4/2/80	12/17/80*	C2-C3
0	985	982	3
10	1015	1013	2
20	2	0	2
30	29	27	2
40	58	57	1
50	86	83	3
60	113	110	3
70	140	138	2
80	169	165	4
90	196	193	3
100	226	221	5
110	255	250	5
120	284	281	3
130	313	309	4
140	342	338	4
150	370	367	3
160	398	395	3
170	424	421	3
180	455	451	4
190	486	482	4
200	516	512	4
210	544	539	5
220	573	569	4
230	603	597	6
240	634	630	4
250	663	660	3
260	692	689	3
270	722	719	3
280	751	747	4
290	781	779	2
300	811	810	1
310	840	839	1
320	868	866	2
330	897	895	2
340	926	924	2
350	955	953	2
Mean	503	500	3
Tape#	1544/12	1544/20	

Table 9. Calibration of bit value versus direction for current meter compass at 31 m. The first column (°T) shows degrees true (0°,90°,180° and 270° denoting north, east, south and west), the next three columns give the bit calibrations at 10° increments on the date shown above the column. The last three columns give the differences between bit calibrations of the columns. The date of the calibration is starred if it was used to process the data for this experiment.

°T	9/26/78	3/25/80*	12/17/80	C2-C3	C4-C3	C2-C4
180	465	470	464	-5	-6	1
190	496	500	492	-4	-8	4
200	526	531	528	-5	-3	-2
210	557	561	560	-4	-1	-3
220	590	594	593	-4	-1	-3
230	619	623	622	-4	-1	-3
240	646	647	647	-1	0	-1
250	675	677	675	-2	-2	0
260	703	706	704	-3	-2	-1
270	730	732	731	-2	-1	-1
280	764	765	766	-1	1	-2
290	796	797	798	-1	1	-2
300	828	829	831	-1	2	-3
310	853	855	856	-2	1	-3
320	882	885	887	-3	2	-5
330	913	913	915	0	2	-2
340	939	940	942	-1	2	-3
350	963	965	967	-2	2	-4
0	983	985	989	-2	4	-6
10	1011	1015	1015	-4	0	-4
20	0	1	3	-1	2	-3
30	24	29	30	-5	1	-6
40	49	53	55	-4	2	-6
50	75	80	79	-5	-1	-4
60	103	107	104	-4	-3	-1
70	130	136	130	-6	-6	0
80	156	161	159	-5	-2	-3
90	185	189	187	-4	-2	-2
100	212	219	213	-7	-6	-1
110	244	249	245	-5	-4	-1
120	276	282	275	-6	-7	1
130	311	318	311	-7	-7	0
140	341	347	335	-6	-12	6
150	371	376	367	-5	-9	4
160	398	403	391	-5	-12	7
170	429	436	421	-7	-15	8
Mean	507	510	508	-4	-3	-1
Tape#	1542/7	1542/9	1542/13			